Beier, C., Haase, K. M., Abouchami, W., Krienitz, M. S., Hauff, F. (2008): Magma genesis by rifting of oceanic lithosphere above anomalous mantle: Terceira Rift, Azores. - Geochemistry Geophysics Geosystems (G3), 9, Q12013

DOI: 10.1029/2008GC002112

MAGMA GENESIS BY RIFTING OF OCEANIC LITHOSPHERE ABOVE ANOMALOUS MANTLE: THE TERCEIRA RIFT, AZORES

Christoph Beier[1,2,3], Karsten M. Haase[4], Wafa Abouchami[1], Marc-S. Krienitz[2,5] and Folkmar Hauff[6]

[1]Max-Planck-Institut für Chemie (Otto-Hahn-Institut), Abteilung Geochemie, Postfach 3060, 55128 Mainz, Germany, Email: cbeier@els.mq.edu.au

[2]Institut für Geowissenschaften, Christian-Albrechts-Universität zu Kiel, Ludewig-Meyn-Straße 10, 24118 Kiel, Germany

[3]National Key Centre for Geochemical Evolution and Metallogeny of Continents (GEMOC), Department of Earth and Planetary Sciences, Macquarie University, NSW 2109, Sydney, Australia

[4]GeoZentrum Nordbayern, Universität Erlangen, Schlossgarten 5, D-91054 Erlangen

[5]GeoForschungsZentrum Potsdam, Telegrafenberg B124, 14473 Potsdam, Germany

[6]IFM-GEOMAR, Leibniz-Institut für Meereswissenschaften, Wischhofstr. 1-3, 24148 Kiel, Germany

[*]corresponding author, present address: National Key Centre for Geochemical Evolution and Metallogeny of Continents (GEMOC), Department of Earth and Planetary Sciences, Macquarie University, NSW 2109, Sydney, Australia, Tel.: +61/2/9850-4405, Fax.: +61/2/9850-8943, Email: cbeier@els.mq.edu.au

ABSTRACT

The Terceira Rift formed relatively recently (~1 Ma ago) by rifting of the old oceanic lithosphere of the Azores Plateau and is currently spreading at a rate of 2-4mm/yr. Together with the Mid-Atlantic Ridge the Terceira Rift forms a triple junction that separates the Eurasian, African and American Plates. Four volcanic systems (São Miguel, João de Castro, Terceira, Graciosa), three of which are islands, are distinguished along the axis and are separated by deep avolcanic basins similar to other ultraslow spreading centres. The major element, trace element and Sr-Nd-Pb isotope geochemistry of submarine and subaerial lavas display large along-axis variations. Major and trace element modelling suggests melting in the garnet stability field at smaller degrees of partial melting at the easternmost volcanic system (São Miguel) compared to the central and western volcanoes, which appear to be characterised by slightly higher melting degrees in the spinel/garnet transition zone. The degrees of partial melting at the Terceira Rift are slightly lower than at other ultraslow Mid-Ocean Ridge spreading axes (Southwest Indian Ridge, Gakkel Ridge) and occur at greater depths as a result of the melting anomaly beneath the Azores. The combined interaction of a high obliquity, very slow spreading rates and a thick pre-existing lithosphere along the axis probably prevents the formation and eruption of larger amounts of melt along the Terceira Rift. However, the presence of ocean islands

requires a relatively stable melting anomaly over relatively long periods of time. The trace element and Sr-Nd-Pb isotopes display individual binary mixing arrays for each volcanic system and thus provide additional evidence for focused magmatism with no (or very limited) melt or source interaction between the volcanic systems. The westernmost mantle sources beneath Graciosa and the most radiogenic lavas from the neighbouring Mid-Atlantic Ridge suggest a mantle flow from Graciosa towards the Mid-Atlantic Ridge, and, hence a flux of mantle material from one spreading axis into the other. The Terceira Rift represents a unique oceanic rift system situated within the thickened, relatively old oceanic lithosphere and thus exhibits both oceanic and continental features.

INTRODUCTION

The Mid-Ocean Ridge (MOR) system represents the largest magmatic feature on Earth with a length of more than 60,000 kilometres. Early studies suggested that the Mid-Ocean Ridges were relatively uniform structures erupting basalts of homogeneous incompatible-element depleted tholeiitic composition [*Gast*, 1968; *Shaw*, 1970]. However, more detailed investigations revealed that both tectonic structures and composition of the rocks of the MOR system are highly variable [*Dupré and Allegre*, 1983; *Geshi et al.*, 2007; *Kane and Hayes*, 1994]. One important factor that influences the ridge's structure is the spreading rate, which can vary from 160 mm/a (full spreading) at the East Pacific Rise to ultraslow spreading rates such as at the Southwest Indian Ridge (SWIR; 12-16 mm/a [*Dick et al.*, 2003]) or the Arctic Gakkel Ridge (8-13 mm/a [*Cochran et al.*, 2003]). Because the thermal structure and the magma budget of the MOR depends on the spreading rate, the degree and depth of partial melting, the MORB compositions are also affected which is generally reflected by variable major and trace element composition of the basalts [*Gast*, 1968; *Shaw*, 1970]. It has also been recognised that MORs are evolving, i.e. the spreading rate varies and ridge segments propagate or become extinct [*Kane and Hayes*, 1994; *MacDonald et al.*, 1991; *Smith et al.*, 2001]. Thus, it is expected that during the evolution of a spreading segment the composition of the magmas change as they are affected by variable mantle sources and spreading regimes. Here, we present geochemical data for a segment of the MOR, which developed from a transform fault into an obliquely ultraslow spreading rift separating old oceanic plateau lithosphere.

The unique setting of the Terceira Rift in the submarine Azores Plateau, with an ultraslow spreading axis above a melting anomaly, allows to address the following fundamental questions: are melting processes and mantle sources homogeneous in the presence of a melting anomaly and, if a heterogeneous mantle is present, are melting processes and mantle source distribution along ultraslow spreading ridges either controlled by rifting, by lithospheric thickness, by mantle temperature or by their composition? This study presents new major element, trace element and Sr-Nd-Pb isotope data from a suite of submarine and subaerial volcanic rocks along the ultraslow spreading Terceira Rift in the Azores. Large scale along-axis geochemical variations suggest deeper melting at the island of São

Miguel, farthest from the Mid-Atlantic Ridge, but relatively small along-axis changes in degrees of partial melting. The occurrence of distinct, well defined mantle source compositions with very limited mixing between the magmatic segments implies that, despite the presence of a melting anomaly, the distribution of magmatic activity and mantle sources along axis is mainly controlled by the spreading movement. The occurrence of small scale heterogeneity also gives evidence that the chemical enrichment of the adjacent Mid-Atlantic Ridge may be the result of mixing between the enriched Graciosa mantle source and a depleted mantle, indicating a flux of mantle material from one spreading axis into the other.

GEOLOGICAL SETTING

The ultraslow (2-4 mm/a) and obliquely spreading Terceira Rift formed very recently [about 1 Ma ago, *Vogt and Jung*, 2004] probably from a transform fault and is rifting old oceanic lithosphere of the northern Azores Plateau (Fig. 1a). Together with the Gloria transform fault in the east, the Terceira Rift forms the plate boundary between the African and Eurasian Plates. Three (i.e. São Miguel, Terceira, Graciosa) of the nine volcanic islands of the Azores Archipelago and the submarine João de Castro seamount are situated along the Terceira Rift. Each volcanic centre is bordered by deep avolcanic basins (Fig. 1b). The volcanically active seamount João de Castro lies between the islands of Terceira and São Miguel and reached subaerial stages in 1638 and 1720 but was eroded soon after [*Nunes et al.*, 2003]. The Azores Plateau probably formed by a melting anomaly in the mantle either as a result of a small thermal plume head [*Cannat et al.*, 1999; *Schilling*, 1975; *White et al.*, 1979] or of anomalously volatile-enriched mantle, a "wetspot" [*Bonatti*, 1990; *Schilling et al.*, 1980]. Seismic tomography studies reveal the presence of mantle with anomalously slow seismic velocities beneath the Azores, but a connection to the lower mantle is disputed [*Courtillot et al.*, 2003; *King*, 2007; *Montelli et al.*, 2004; *Ritsema and Allen*, 2003]. In fact, the lack of a tail of the mantle anomaly has been interpreted to possibly show a dying plume with a short life time of less than 40 Ma [*Silveira et al.*, 2006]. Lavas from São Miguel and Terceira have relatively primitive He and Ne isotope compositions which indicate the presence of relatively un-degassed mantle material beneath the Azores [*Madureira et al.*, 2005]. It was suggested that mantle material from beneath Terceira is flowing into the MAR causing the geochemical anomaly at the spreading centre [*Moreira et al.*, 1999b].

GPS and laser measurements show that the islands lie in an extensional regime [*Miranda et al.*, 1998]. Based on relative plate motions using the NUVEL-1A model, *Vogt and Jung* [2004] determined spreading rates of 2-4 mm/a for the recent plate boundary between the Eurasian and African Plates. Such ultraslow extensional movements are comparable to those observed at continental rifts like, for example, the East African Rift [*Corti*, 2008; *Ebinger et al.*, 1993]. Extensional tectonics in the Terceira Rift are also revealed by magnetic anomalies [*Searle*, 1980], geometric modelling [*Krause* *and Watkins*, 1970], and by extensional tectonic structures on some islands, e.g. at the western end of São Miguel [*Beier et al.*, 2006]. The Terceira Rift and the MAR form the Ridge-Ridge-Ridge plate triple junction between the three bordering plates (Fig. 1). Although the precise location of this triple junction is not well defined, focal earthquake mechanisms infer the locus W of Faial and/or Graciosa [*Grimison and Chen*, 1986; 1988; *Udias et al.*, 1976].

METHODS

SAMPLING AND SAMPLE TREATMENT

The submarine samples were obtained during two cruises with the German research vessel POSEIDON in 1997 (POS 232) and in 2002 (POS 286). The islands of São Miguel, Terceira and Graciosa were sampled during three field-trips between 2001 and 2003.

Most submarine samples dredged along the Terceira Rift are fresh and only few are slightly hydrothermally altered. Volcanic glasses were dredged west of São Miguel, at João de Castro and west of Graciosa. Representative samples have been studied petrographically. Wherever possible glass was separated, hand-picked, washed and used for the geochemical analyses. Fresh cores were cut from samples without glass, coarse crushed, washed thoroughly in deionised water, and then fine crushed in an agate ball mill.

Major element analyses on whole rocks were carried out on a Philips 1400 XRF spectrometer at the Institut für Geowissenschaften, Universität Kiel using fused glass beads. Results for all samples and international rock standards are presented in supplemental Table 1 and show that precision and accuracy are better than 0.8 % (2σ) and 1 % (2σ), respectively. The major element analyses of glasses were determined on a JEOL JXA8900 Superprobe electron microprobe at the Institut für Geowissenschaften, Universität Kiel. SiO_2, TiO_2, Al_2O_3, FeO^T, MnO, MgO, CaO, Na_2O, K_2O, P_2O_5, Cr_2O_3 and, in some cases, also F, Cl and NiO were measured. The EMP operated with an accelerating voltage of 15 kV, a beam current of 12 nA and a defocused beam (12µm). Counting times were set to 20 and 10 seconds for peaks and backgrounds, respectively.

Trace element analyses were carried out using an Agilent 7500c/s Quadrupole Inductively Coupled Plasma Mass Spectrometer (ICP-MS) at the Institut für Geowissenschaften, Universität Kiel. The samples were prepared following procedures in *Garbe-Schönberg* [1993]. Trace element analyses of the samples along with international rock standards are reported in supplemental Table 1, and indicate a standard deviation of the precision and accuracy of <5% and <8% (2σ), respectively, based on repeated standard measurements.

Sr-Nd-Pb isotope analyses were performed at the Max-Planck-Institut für Chemie in Mainz (MPI) and at IFM-GEOMAR in Kiel. In both labs ~150-200 mg of sample grains were leached in hot 6N HCl for two hours, ultrasonicated 30 minutes and then dissolved using standard digestion procedure described by *Eisele et al.* [2002] and *Abouchami et al.* [2000a]. At the MPI Sr and Nd isotopes were measured on a Finnigan MAT 261 (TIMS) and a Nu Plasma (HR MC-ICP-MS), respectively, while at IFM-GEOMAR, Sr and Nd compositions were both measured on a TRITON TIMS. Sr and Nd isotope ratios on all instruments were obtained in static mode and mass bias corrected relative to $^{86}Sr/^{88}Sr$= 0.1194 and $^{146}Nd/^{144}Nd$= 0.7219. In Mainz, standard runs of NIST SRM-987 (formerly NBS 987) gave 0.710299 ±26 (2SD, n= 16) while SRM 987 gave 0.710273 ±5 (n= 8) in Kiel. Sr isotope analyses were normalised to a common value of 0.710250 for NIST SRM-987. La Jolla Nd standard measured on the Nu Plasma HR MC-ICP-MS in Mainz yielded a value of 0.511862 ±24 (n= 14). The data obtained in Mainz were mass fractionation corrected using the generalised power law from the exponential law. In Kiel, the in-house Nd monitor SPEX yielded $^{143}Nd/^{144}Nd$ = 0.511710 ±5 (n= 5) corresponding to a La Jolla value of 0.511845 ±6 (n =161). The Nd isotope ratios in Kiel were normalised to a common value of La Jolla 0.511858. Procedural blanks in both laboratories were generally better than 0.2 ng and 0.1 ng for Sr and Nd, respectively.

High precision Pb isotope analyses were carried out at the Max-Planck-Institut für Chemie in Mainz, using the triple spike technique [*Galer and Abouchami*, 1998; *Galer*, 1999]. Samples were loaded onto Re filaments with a silica-gel H_3PO_4 activator and unspiked and spiked sample aliquots were measured on a TRITON TIMS in static multicollection mode. The mass bias-correction estimated from the two runs follows the method outlined in *Galer* [1999]. Based on sample duplicate analyses, the external reproducibility is ~160 ppm for $^{206}Pb/^{204}Pb$, $^{207}Pb/^{204}Pb$, and $^{208}Pb/^{204}Pb$. Standard runs of NBS981 (n = 32) gave average values of 16.9434 ±25, 15.5010 ±24, and 36.7304 ±63 for $^{206}Pb/^{204}Pb$, $^{207}Pb/^{204}Pb$ and $^{208}Pb/^{204}Pb$ respectively. A subset of Pb samples were analysed on a Finnigan MAT 262 TIMS at IFM-GEOMAR using an external mass bias correction based on repeated NBS981 measurements. The long-term reproducibility in this lab for NBS981 (n =189) is $^{206}Pb/^{204}Pb$ = 16.899 ±7, $^{207}Pb/^{204}Pb$ = 15.437 ±9, $^{208}Pb/^{204}Pb$ = 36.525 ±29. These values were normalized to the Mainz NBS981 triple spike values to obtain mass bias factors applied to the sample data. Although conventional Pb isotope data cannot resolve small scale variations, the large Pb isotopic variation in this particular sample set allows to merge both datasets. Representative major element, trace element, and Sr-Nd-Pb isotope data are given in Table 1. A comprehensive dataset is available in supplemental Table 1.

RESULTS

Major and trace elements

The Terceira Rift lavas are subdivided into four groups representing the volcanic centres of São Miguel, João de Castro (including lavas from the neighbouring Hirondelle Basin, Fig. 1), Terceira and Graciosa and range from alkali basalts to trachytes on a Total Alkali versus Silica (TAS diagram; Fig. 2). The two major islands of São Miguel and Terceira display different trends with the São Miguel lavas being more alkaline (Fig. 2), due to their slightly higher K_2O-contents (see below). A few samples also plot in the basanite and phonotephrite fields. Most samples from the João de Castro seamount overlap the field of the São Miguel lavas whereas the Graciosa samples are relatively primitive (most have >6 wt.% MgO) overlapping the Terceira and São Miguel fields (see Fig. 3). Here, we will concentrate on the more primitive lavas with MgO contents higher than 5 wt.% in order to determine magma generation and source processes in the mantle.

The SiO_2 contents in the lavas from São Miguel, João de Castro, Terceira and Graciosa are relatively constant at 46±3 wt.% in the range between 15 and 5 wt.% MgO (Fig. 3a). The FeO^T, Na_2O, (Fig. 3c, f) and CaO (not shown) contents slightly increase with decreasing MgO in the primitive lavas from the four volcanic systems of the Terceira Rift and follow narrow trends (Fig. 3) which resemble the well-defined trend of lavas from Sete Cidades volcano on São Miguel [*Beier et al.*, 2006]. In terms of the Al_2O_3 contents we find that Graciosa has significantly higher concentrations compared to the other three volcanic systems which lie on one trend of increasing Al_2O_3 with decreasing MgO (Fig. 3b). The most primitive lavas with MgO >8 wt.% also display differences in FeO^T, with Graciosa, Terceira and João de Castro having slightly lower FeO^T contents at a given MgO than São Miguel lavas. TiO_2 concentrations increase from 18 to about 5 wt.% MgO and are generally lower in basalts from Graciosa and Terceira compared to lavas from São Miguel and João de Castro. The most significant differences among the Terceira Rift lavas exist for K_2O with the São Miguel and João de Castro lavas having higher K_2O contents at a given MgO than lavas from the western two volcanic systems Terceira and Graciosa (>9 wt.% for Graciosa specifically, Fig. 3e). Similarly, the São Miguel and João de Castro samples are also more enriched in other highly incompatible elements like Rb, Ba and Ce.

The trace element patterns of the primitive lavas (MgO >5 wt.%) from the four volcanic systems of the Terceira Rift lavas are relatively similar with Th, U, K and Pb troughs and peaks in Rb, Ba, Nb, Ta and La. The most notable difference is that the São Miguel and João de Castro lavas have higher enrichments of the light REE relative to the heavy REE contents than lavas from the two western Terceira Rift volcanic systems (Figs. 4 and 5a). For example, the eastern two structures generally have $(Ce/Yb)_N \geq 9$ in contrast to the Terceira and Graciosa lavas which have $(Ce/Yb)_N \leq 9$ (see discussion below and Fig. 8). The samples from Terceira, Graciosa and João de Castro Seamount have relatively narrow variations of $(Ce/Yb)_N$ of 6-9, 7-10 and 9-10, respectively, but the São Miguel lavas vary between 9 and 17, i.e. nearly by a factor of two. Although only three samples from João de Castro have >5 wt.% MgO they resemble São Miguel lavas in terms of $(Ce/Yb)_N$ but have relatively low $(Dy/Yb)_N$ similar to basalts from the western islands. In contrast, São Miguel basalts have the highest $(Dy/Yb)_N$ but the Yb contents in the near-primary magmas are comparable in all lavas suites (1.5-1.7 ppm). Graciosa and Terceira both generally exhibit peaks in Ti (with the exception of very few samples for Terceira which have a slight Ti trough). Lavas from the João de Castro seamount and many samples from São Miguel also have higher Rb/Nb ratios than the rocks from Graciosa and Terceira (Fig. 5). On the other hand, the variations in the Heavy Rare Earth Elements (HREE) and Nb/Zr are not as clear although primitive São Miguel lavas show higher $(Dy, Tb/Yb)_N$ ratios than the other lava groups (Fig. 5). Although they overlap, the Terceira lavas tend towards slightly lower Nb/Zr and Th/U (Fig. 5) than the lavas from São Miguel and João de Castro, implying different mantle source compositions along the Terceira Rift.

Radiogenic isotope compositions

The large variation of Sr, Nd and Pb isotope compositions in the lavas from São Miguel is long known and the origin of their distinct mantle sources has been discussed elsewhere [*Beier et al.*, 2007; *Widom et al.*, 1997] and thus will not be discussed in detail here. Lavas from the other three volcanic systems of the Terceira Rift show relatively constant Sr isotope ratios between 0.7033 and 0.7036 but highly variable and distinct $^{143}Nd/^{144}Nd$ (Fig. 6a). Thus, the lowest $^{143}Nd/^{144}Nd$ occur in rocks from João de Castro, slightly higher $^{143}Nd/^{144}Nd$ ratios at Graciosa and the most radiogenic $^{143}Nd/^{144}Nd$ in lavas from Terceira (Fig. 6a). Importantly, each volcanic system of the Terceira Rift forms a distinct trend in the Sr-Nd-Pb isotope space (Fig. 6). The São Miguel lavas show the largest Sr-Nd-Pb isotopic variations and resemble some Graciosa lavas at unradiogenic $^{87}Sr/^{86}Sr$. The Pb-Pb isotope systematics reveals complex variations for each volcanic system where they form distinct arrays with different slopes (Fig. 6d and e). São Miguel lavas show the largest Pb isotopic variations with $^{206}Pb/^{204}Pb$ ranging from 19.3 to 20.2 that form steep, positive arrays towards high $^{207}Pb/^{204}Pb$. João de Castro and Terceira/Graciosa each have distinct Pb isotopic trends. Lavas from João de Castro have the lowest Pb isotope ratios of the Terceira Rift volcanoes and also the lowest $^{143}Nd/^{144}Nd$ (Fig. 6f). The low $^{206}Pb/^{204}Pb$ and Sr isotope compositions of lavas from João de Castro resemble North Atlantic MORB but have significantly lower $^{143}Nd/^{144}Nd$, and also lower $^{207}Pb/^{204}Pb$ for a given $^{206}Pb/^{204}Pb$ than MORB. Graciosa lavas have slightly more radiogenic $^{208}Pb/^{204}Pb$ and $^{207}Pb/^{204}Pb$ ratios at a $^{206}Pb/^{204}Pb$ range comparable to Terceira but converge at the highest $^{206}Pb/^{204}Pb$ (Fig. 6d and e). On a $^{143}Nd/^{144}Nd$ diagram all lavas of the Terceira Rift (except São Miguel) lie on a broad positive correlation (Fig. 6f), while São Miguel forms a well correlated array, orthogonal to the other Terceira Rift lavas. Importantly, the trends of the different volcanic systems of the Terceira Rift as well as the MAR converge at a composition with $^{87}Sr/^{86}Sr$ ~0.7035, $^{143}Nd/^{144}Nd$ ~0.5129 and $^{206}Pb/^{204}Pb$ of 19.5 which has been associated with a mantle component termed FOZO [*Hart et al.*, 1992], recently re-defined by *Stracke et al.* [2005], or "C" [*Hanan and Graham*, 1996]. This composition is represented most clearly by some lavas from Graciosa and those from the western end of São Miguel, but appears to be inherent in all Terceira Rift magmas. This mantle source also affects the adjoining MAR from ~37° to 40°N [*Dosso et al.*, 1999] leading to enriched incompatible element and Sr-Nd-Pb isotope compositions in MORB from this region.

DISCUSSION

MAGMA GENERATION ALONG THE TERCEIRA RIFT

Because most of the lavas of the different Terceira Rift volcanoes lie on distinct narrow trends of major and trace elements vs. MgO contents (Figs. 2-5) we conclude that each suite of rocks represents a liquid line of descent. In general, these trends resemble those observed for the well-studied Sete Cidades volcano on São Miguel and thus we follow the arguments of Beier et al. [2006] suggesting that the Terceira Rift primary magmas may have about 12.5 wt.% MgO. Lavas with >12.5 wt.% MgO are considered to be the result of the accumulation of olivine and clinopyroxene, because many of these lavas contain olivine and clinopyroxene xenocrysts [see also discussion in *Beier et al.*, 2006] while lavas with <5 wt.% MgO do show evidence for the extensive crystallisation of plagioclase and Fe-Ti oxides similar to Sete Cidades volcano on São Miguel. Thus, for each volcanic system we determine an approximate primary magma composition from the major element trends in Figure 3 for all lavas with >5 wt.% MgO. We have estimated the primary magma composition to be in equilibrium with mantle olivine (Fo89), i.e. the primary magmas have Mg# ~72 [*Niu and O'Hara*, 2008; *Roeder and Emslie*, 1970]. In Table 2 the compositions of these estimated primary magma compositions for each volcanic system of the Terceira Rift are listed. These compositions are compared to primary magmas from other oceanic and intraplate and rift lavas and the degree and depth of partial melting can be modelled using both major elements and trace element ratios (Fig. 7). The major elements SiO_2, Al_2O_3 and FeO^T can provide information about variations in melting depth using experimental data from dry peridotite [e.g. *Hirose and Kushiro*, 1998] and pyroxenite [e.g., *Hirschmann et al.*, 2003; *Kogiso et al.*, 1998]. The relatively high Al_2O_3 and low SiO_2 of the Graciosa magma suggests melting of peridotite at pressures of about 3 GPa (i.e. an average depth of ~90 km) and relatively low temperatures whereas Terceira magmas formed at higher degrees of melting and probably also higher temperatures but comparable pressure. Interestingly, the Graciosa magmas resemble primitive basalts from the Heimaey volcanoes [*Mattsson and Oskarsson*, 2005], i.e. a propagating rift into >3 Ma-old Icelandic crust and thus from a comparable young setting [see *Mattsson and Hoskuldsson*, 2003, and references therein].

The São Miguel primary magmas have lower Al_2O_3 and SiO_2 than the Terceira magmas which implies higher pressures of partial melting (Fig. 7). Lower concentrations of Al_2O_3 in the São Miguel basalts could also give evidence for the presence of increased amounts of residual garnet [*Herzberg*, 1995; *Herzberg and O'Hara*, 1998]. The amount of garnet will either be controlled by a change of mantle lithology, e.g. the presence of garnet pyroxenite veins or by increasing depth of melting, and, hence, increased amounts of residual garnet. If the higher HREE ratios at São Miguel would be solely attributed to the presence of garnet pyroxenite veins [see discussion in *Hirschmann and Stolper*, 1996], the Al_2O_3 contents would be significantly increased, because a garnet peridotite lithology contains approximately 8 wt.% garnet [*Salters and Longhi*, 1999; *Salters et al.*, 2002], whereas pyroxenite may contain up to 20 wt.% garnet [*Hirschmann and Stolper*, 1996]. Partial melting of garnet pyroxenite would thus lead to high Al_2O_3 contrary to the observed low concentrations of the Terceira Rift magmas (Fig. 7). We therefore conclude that the Graciosa, João de Castro and some of the Terceira magmas have formed at lower pressures possibly ranging into the spinel stability field whereas those from those from São Miguel were generated in the garnet stability field at pressures of ~4 GPa (120 km depth, Fig. 7). This is in agreement with thickening of the lithosphere towards the east, i.e. with increasing distance from the MAR. It also implies that the oceanic lithosphere is largely intact and that neither rifting nor re-heating by the Azores plume did thin it significantly. The ages of the oceanic crust beneath the Terceira Rift volcanoes ranges from about 10 Ma beneath Graciosa [*Cannat et al.*, 1999] to about 45 Ma beneath São Miguel [*Searle*, 1980]. Consequently, the depth of the 1300°C isotherm for a normal oceanic spreading centre increases from 35 to 80 km, respectively which is in agreement with melting in the garnet stability field beneath the eastern volcanoes. In contrast, a significant part of the melting column beneath Graciosa and Terceira lies in the spinel stability field because the spinel-garnet transitions occurs between 70 to 80 km depending on the mantle lithology [*Robinson and Wood*, 1998]. The fact that the lithosphere of the Azores Plateau formed by increased amounts of partial melting due to the presence of a melting anomaly could have additionally thickened the lithosphere, however, the increasing lithospheric thickness from the MAR and the consistency between the estimated depth of the 1300°C isotherm and geochemical data suggests that the influence of the melting anomaly may indeed be small.

The degree of partial melting beneath the Terceira Rift can be estimated using TiO_2 rather than Na_2O because experiments have shown that Na partitioning in clinopyroxene is pressure-dependent with D_{Na} increasing with increasing pressure [*Blundy et al.*, 1995]. In contrast, Ti is not affected by variable pressures. On the basis of variable TiO_2 in the Azores magmas it has been argued that São Miguel basalts formed by lower degrees of melting than magmas from the western volcanoes like those from Pico Island [*Prytulak and Elliott*, 2007]. Indeed, we find a variation of TiO_2 contents with the São Miguel and João de Castro primary magmas having high TiO_2 of about 2.7 compared to about 2.1 in the Graciosa and Terceira magmas, respectively (Fig. 8a). On the other hand, the estimated primary magmas from both eastern and western volcanoes have comparable Na_2O between 2.1 and 2.6 wt.%. A slightly lower degree of partial melting beneath São Miguel and João de Castro seamount is supported by their higher enrichment of light and middle REE relative to Yb (Figs. 4 and 8).

Alternatively, the relatively enriched Ti contents of the São Miguel and Graciosa lavas at similar Na contents as the remaining Terceira Rift lavas could be due to an increased Ti concentration in the mantle source relative to Na. If an increased Ti content in the mantle source would be responsible for this signature, Ti has to be enriched by a factor of ~1.5 relative to the Na concentration to produce the observed trend assuming the same modal composition for all Terceira Rift mantle sources. An enrichment of Ti has also been proposed by Prytulak and Elliott [2007] who argue for the presence of an enriched component from recycled oceanic crust in peridotitic mantle. We agree that a possible mechanism to explain the combined higher Ti at slightly lower Na contents of the São Miguel and possibly also Graciosa lavas may likely be the presence of an alkaline component, e.g. recycled, subducted oceanic crust which will have a higher Ti but less increased Na contents. In Beier et al. [2007] we have argued for the presence of recycled oceanic crust in the São Miguel lavas. Whereas recycled oceanic crust will be mainly of pyroxenitic and/or eclogitic composition [see *Stracke et al.*, 1999 and references therein], most major elements and REE will be largely unaffected by changes in mantle lithology, i.e. the changes observed in Ti are too large to be solely explained by varying amounts of pyroxenite beneath the Terceira Rift. However, to ensure the best possible fit we have modelled the trace element and REE systematics (see below) considering the presence of pyroxenite.

Modelling the Na and Ti contents and REE contents of the Terceira Rift lavas (Fig. 8a) using the batch-melting equation [*Shaw*, 1970] shows that the Ti-Na compositional variability of the axis lavas may indeed best be explained by mixing small amounts (~10-20%) of an alkali basaltic component mixed with a depleted upper mantle leaving the REE concentrations relatively unaffected (Fig. 8b & c, Table 3). The presence of an alkaline component, i.e. an enriched, recycled oceanic crust, in the São Miguel mantle sources has been previously suggested based on quantitative trace element and Sr-Nd-Pb-Hf isotope modelling [*Beier et al.*, 2007; *Elliott et al.*, 2007].

Estimates on the degree of partial melting using REE modelling are generally similar to those derived from the Ti-Na systematics (Fig. 8a). The Ce/Yb versus Ce systematics are positively correlated in the Terceira Rift samples indicating a slightly increasing degree of partial melting from São Miguel (lowest) over Graciosa (intermediate) to highest degrees of partial melting beneath Terceira with the lowest Ce/Yb ratio (Fig. 8b) as already inferred from the variations in La/Sm ratios (Fig. 5). Because the MREE and HREE are most sensitive to varying amounts of garnet, we will also use the even more incompatible trace elements to confirm the observations made by the La/Sm ratios. Our model suggests that the elevated Dy/Yb of the São Miguel and some Terceira lavas formed by partial melting under the influence of higher amounts of garnet (~15%) whereas the lower Dy/Yb of the western islands of Graciosa, some lavas from Terceira and lavas from João de Castro (Fig. 8c) formed by melting of mantle containing ~10 % residual garnet and 5% spinel, i.e. at the transition from garnet to spinel stability field. It has to be noted though that the lavas from Terceira are being considered to have both low and high Dy/Yb ratios (Fig. 8c). To account for the possible presence of pyroxenite in the Azores mantle sources we assume equal amounts of pyroxenite and peridotite (see figure caption of Figure 8 for details) to ensure the best possible fit. While the REE ratios (Fig. 8b and c) and the presence of recycled oceanic crust imply that pyroxenitic veins may be present beneath the Azores, the Al_2O_3 contents at given SiO_2 contents (Fig. 7) are too low to be solely explained by pyroxenite melting. The discrepancy between major and trace elements may possibly be best explained by re-equilibration of the melts with the surrounding mantle leaving the trace elements relatively unaffected while the major elements are re-equilibrated. If the modal source compositions are largely similar then the magmas from São Miguel and João de Castro have formed by slightly smaller degrees of partial melting (1-2%) than the melts beneath the western Terceira Rift ranging from 2 to 4% (inferred from the REE ratios in Figs. 8b and c).

We conclude that the magmas generated beneath Graciosa, Terceira and João de Castro have been generated in the garnet/spinel transition zone in contrast to the magmas beneath São Miguel which formed in the garnet stability field, only. The degrees of partial melting along the axis indicate that, in general, the eastern volcanoes (São Miguel particularly) have slightly lower degrees of partial melting than the western islands (Terceira and Graciosa), however, these changes are small. Along the oblique spreading segments of the SWIR decreasing degrees of partial melting have been associated with an increasing lithospheric thickness [*Standish et al.*, 2008].

The increasing depth of partial melting towards São Miguel is consistent with an increasing lithospheric thickness with distance from the MAR [e.g., *Cazenave*, 1984]. The age of the lithosphere in the vicinity of the Princessa Alice bank has been estimated to be 10 Ma [*Cannat et al.*, 1999] whereas the lithosphere south of the island of Terceira may be 36 Ma old and the junction between the Terceira Rift and the lateral Gloria fault east of the Azores plateau has been estimated to be 53 Ma [*Searle*, 1980]. Based on these ages the thickness of the oceanic lithosphere can be calculated yielding thicknesses of 36, 68 and >81 km, respectively [*Stein and Stein*, 1992]. However, the formation of alkali basaltic melts beneath the Terceira Rift implies relatively higher pressures of melting than on other ultraslow spreading axes where tholeiitic basalts form by low degree melting at shallow depth such as the SWIR (N-MORB to E-MORB ~7-14% degree of partial melting depending on mantle lithology, [*Standish et al.*, 2008]) or the Arctic Gakkel Ridge [~5%, *Hellebrand and Snow*, 2003]. Higher pressures of melting at the Terceira Rift compared to the other ultraslow spreading axes are a result of young (<6 Ma) rifting of lithosphere formed at the MAR. This lithosphere is probably still largely intact and not yet thinned by the very slow extension (~4 km/Ma). Airy compensation models suggest that the lithosphere beneath the Azores is indeed thickened rather than thinned by mantle melting [*Grevemeyer*, 1999]. Thus, although the mantle beneath the Azores may be either relatively hot and/or volatile-rich material and begins to melt at great depth, the lithospheric lid above the melting zone prevents increased degrees of partial melting.

Mantle Sources and Mixing Along the Terceira Rift

The linear Pb isotope arrays of Graciosa, João de Castro and Terceira either reflect true isochrons or binary mixing lines (Fig. 6d and e). The isotopic array of São Miguel has been modelled to represent a mixing array [*Beier et al.*, 2007]. The results from reduced chi-squared regression lines of the triple spike data indicate a slope of 0.087±0.005 for the João de Castro lavas which is comparable to the slope at Terceira (0.084±0.004) in the $^{207}Pb/^{204}Pb$ versus $^{206}Pb/^{204}Pb$ space (Fig. 6d). If these slopes represent isochrons the corresponding ages would be 1.37±0.12 and 1.31±0.09 Ga, respectively. A calculated regression line from Graciosa gives a slope of 0.009±0.006, representing a zero-age isochron slope giving evidence that the Graciosa samples most likely represent binary mixing rather than an isochron. If the $^{207}Pb/^{204}Pb$-$^{206}Pb/^{204}Pb$ regression lines of João de Castro and Terceira are mantle isochrons this should be also the case for the linear arrays in the $^{208}Pb/^{204}Pb$ versus $^{206}Pb/^{204}Pb$ space. Hence, the inferred source κ ($^{232}Th/^{238}U$) values from the measured Th and U (κ_{TE}) concentrations and from the $^{208}Pb/^{206}Pb$ ratios (κ_{ISO}) should be correlated, i.e. the κ_{TE} should be equal or higher than the κ_{ISO} if due to melting [*Beattie*, 1993]. In contrast to the prediction the κ_{TE} values of João de Castro and Terceira are considerably lower than the κ_{ISO} which is inconsistent with the expected Th/U fractionation during melting [*Abouchami et al.*, 2000a]. Therefore, we suggest that the linear arrays in the $^{207}Pb/^{204}Pb$-$^{206}Pb/^{204}Pb$ and $^{208}Pb/^{204}Pb$-$^{206}Pb/^{204}Pb$ isotope systems do not represent mantle isochrons as a result of mantle melting but more likely reflect mixing lines between two distinct mantle sources on each array.

Two different magma groups along the Terceira Rift can be distinguished based on their K_2O contents with Terceira and Graciosa lavas having lower K_2O than those from São Miguel and João de Castro at a given MgO content (Fig. 3). These two groups can be also distinguished in terms of Nb/Zr and Th/U (Fig. 5) suggesting that the eastern volcanoes of the Terceira Rift have more enriched mantle sources than the western volcanoes. A broad negative correlation between the $^{143}Nd/^{144}Nd$ isotope ratios and the K concentrations (and ratios such as K/Ti, K/U) confirms that these variations are mainly the result of mantle source signatures. However, each single mixing array (Graciosa, São Miguel, João de Castro and Terceira) in the Pb-Pb isotope spaces gives evidence for two component mixing between discrete mantle end-members (dashed circles in Figs. 6d and e). All mixing arrays, except João de Castro appear to converge to a common Azores composition that is reflected by the unradiogenic Graciosa samples. The source of the João de Castro seamount lavas mixes with a relatively unradiogenic mantle source different from basalts from the Mid-Atlantic Ridge as indicated by their lower $^{207}Pb/^{204}Pb$ at a given $^{206}Pb/^{204}Pb$ and less radiogenic $^{143}Nd/^{144}Nd$ (Fig. 6d-f). At Graciosa and Terceira the common end-member is characterised by radiogenic Pb isotope ratios and high Nd isotope ratios, in that sense comparable to the HIMU ocean island lavas (high μ =high $^{238}U/^{204}Pb$) such as St. Helena [e.g., *Zindler and Hart*, 1986]. The linear array at Graciosa covers a comparable $^{206}Pb/^{204}Pb$ range as the Terceira lavas but the shallower Graciosa array results from slightly more radiogenic $^{208}Pb/^{204}Pb$ and $^{207}Pb/^{204}Pb$ ratios which is also reflected in higher $^{208}Pb^*/^{206}Pb^*$ ratios at Graciosa than at Terceira (Fig. 6b). The radiogenic Pb end-member compositions of Terceira and Graciosa suggest interaction between the two systems but their relatively unradiogenic Pb end-member compositions indicate that the two unradiogenic mantle sources are slightly distinct, i.e. the common source of the Terceira Rift lavas shows some variation.

The isotope ratios of Sr and Nd are broadly correlated with the La/Sm, Rb/Nb, Ba/Rb, Th/Nb and Th/U ratios (not shown), i.e. generally the lavas with the highest $^{143}Nd/^{144}Nd$ from Terceira also have the highest Sm/Nd but lavas from São Miguel have both, variable Sm/Nd and $^{143}Nd/^{144}Nd$ suggesting that partial melting processes probably affected the Sm/Nd ratio. Although the linear arrays of the Graciosa, Terceira and western São Miguel samples meet at similar ratios in the isotope spaces, the combined trace element (K, Th/U, Ba/Nb, Nb/Zr) and Sr-Nd-Pb isotope systematics (Fig. 9) show that each volcano along the axis contains its own isolated mantle source implying significant heterogeneity in the mantle beneath the Azores on a scale of about 100 km. The limited mixing between different sources has also been observed on a much smaller scale of about 20 km between the western and eastern volcanoes at São Miguel [*Beier et al.*, 2007; *Haase and Beier*, 2003].

Our new data reveal that, rather than the three end-members in the Azores lavas suggested by previous authors [e.g., *Moreira et al.*, 1999b], at least four end-members are required to explain the isotopic variation of the Terceira Rift lavas. The three end-members were previously believed to be MORB, a plume component represented by Terceira lavas, and an enriched mantle component represented by lavas from eastern São Miguel [e.g. *Beier et al.*, 2007; *Elliott et al.*, 2007]. The isotopic variation observed in each volcanic system indicates that at least two sources are present beneath each structure. Some of the lavas from Graciosa with $^{87}Sr/^{86}Sr$ of ~0.7035, $^{143}Nd/^{144}Nd$ of ~0.5129 and $^{206}Pb/^{204}Pb$ of ~19.4 to 19.6 appear to represent a possible end member common in all other volcanic systems as well as MORB and thus could be an average "Azores plume component". Interestingly, this source also resembles the composition suggested for the FOZO or "C" component which is believed to be abundant in the mantle [*Hanan and Graham*, 1996; *Hart et al.*, 1992; *Stracke et al.*, 2005]. While the origin of this common component in the Azores is beyond the scope of this work, the data clearly require the Azores mantle anomaly to be heterogeneous on a scale of tens of kilometres similar to findings in mantle plumes like Hawaii [*Abouchami et al.*, 2000b]. The low degrees of partial melting (<5%) of the Terceira Rift magmas may be responsible for the preferred sampling of small heterogeneities as a result of the increased viscosity of low degree melts at relatively lower temperatures compared to higher degree melts at higher temperatures [*Bourdon et al.*, 2006; *Scarfe and Cronin*, 1986].

INFLUENCE OF THE TERCEIRA RIFT MANTLE ON MID-ATLANTIC RIDGE BASALTS

The existence of a geochemical anomaly in the lavas erupting at the Mid-Atlantic Ridge close to the Azores is long known [e.g. *Bougault and Treuil*, 1980; *Schilling*, 1975; *White et al.*, 1975; *White et al.*, 1976] and has been attributed to the influx of enriched and hot mantle that originates from a deep mantle plume beneath the Azores. Relatively primitive He isotope ratios ($^{4}He/^{3}He$ ~64,000) from Terceira and the adjacent MAR have been interpreted to result of plume-ridge interactions between the plume centre located beneath Terceira and the MAR [*Moreira et al.*, 1999a]. However, we have shown that the lavas from Terceira and Graciosa resemble each other in $^{206}Pb/^{204}Pb$ compositions but significant differences exist in $^{207}Pb/^{204}Pb$, $^{208}Pb/^{204}Pb$ and $^{143}Nd/^{144}Nd$ ratios (Fig. 6). Thus, the Terceira lavas have too high $^{143}Nd/^{144}Nd$, and too low $^{207}Pb/^{204}Pb$ to represent the mixing end member for Mid-Ocean Ridge Basalts (MORB) from the adjacent MAR (Fig. 6d-f) and rather, the material influencing the spreading axis has a composition comparable to the Graciosa mantle source. In fact, despite slight offsets, the unradiogenic Graciosa lavas lie closest to the point of convergence of the trends of all Terceira Rift and MAR lavas suggesting that they could possibly represent a common mantle end member inherent in all Terceira Rift magmas as well as MORB close to the Azores. The $^{143}Nd/^{144}Nd$ and $^{206}Pb/^{204}Pb$ similarities between the MAR and Graciosa suggest mixing of the Graciosa mantle source into the MAR mantle, and thus indicates a mantle flux from Graciosa towards the MAR. This seems also evident from the bathymetry in Figure 1, i.e. there is no bathymetrical evidence for active volcanism between the dredged seamount west of Graciosa and the MAR. If the melts are focused along the Terceira Rift (see discussion below) then they will likely be also focused into the MAR and/or towards Graciosa, respectively. As no He isotope measurements are known from Graciosa and the origin of the primitive He isotopic composition are still a matter of debate, we suggest that the enriched MAR signature is a result of mantle flux from Graciosa to the MAR. We speculate that Graciosa's lavas with the lowest Pb isotope ratios will also have the most primitive He isotope ratios, however this has to be tested.

Because Graciosa is the island closest to the MAR its influence on the spreading axis is not surprising. However, we note that no plume centre can be defined in the Azores because five of the islands east of the MAR have erupted in historical times (São Miguel, Terceira, Graciosa, Faial, Pico) and with one exception all islands (Santa Maria) east but also west of the MAR are very young (2-0.1 Ma) [*Abdel Monem et al.*, 1975; *Calvert et al.*, 2006; *Féraud et al.*, 1980; *Féraud et al.*, 1981; *Johnson et al.*, 1998; *Madeira et al.*, 1995; *McKee and Moore*, 1992; *Snyder et al.*, 2007], implying that there is no age progression. Because the young volcanism along the Terceira Rift is a result of extension it appears possible that the centre of an actively ascending deep mantle plume lies beneath Graciosa-São Jorge-Faial-Pico, the islands closest to the MAR which could also explain the volcanism of the latter two islands. However, such a model cannot explain why two very young volcanic islands Corvo and Flores formed west of the MAR because the relatively deep and thin crust of the MAR implies that there is most likely no plume rising beneath the MAR [*Cannat et al.*, 1999]. Some tomographic models suggest that there is no connection of the Azores mantle anomaly into the deep mantle [*Courtillot et al.*, 2003; *Ritsema and Allen*, 2003] and thus this material may represent old material from a plume head arriving beneath the lithosphere some 10 to 5 Ma ago but which is no longer active, hence there is no evidence for an ascending tail of a mantle plume [*Ritsema and Allen*, 2003; *Silveira et al.*, 2006]. In this case the fossil plume head material may flow into the MAR spreading axis and the Terceira Rift because it is less viscous and less dense than the upper mantle material and because of the suction of the diverging plates. The presence of 5-10 Ma-old mantle plume head material beneath the whole Azores Platform and west of the MAR may also explain the young volcanism of the two islands west of the MAR by passive melting of enriched material within the mantle anomaly.

COMPARISON TO ULTRASLOW RIDGES AND CONTINENTAL RIFTS

The Terceira Rift is characterised by an avolcanic-volcanic segmentation pattern (Fig. 1b) that has been also observed along the oceanic Southwest Indian (SWIR [*Sauter et al.*, 2004a]) and Arctic Gakkel Ridges [*Michael et al.*, 2003] and the continental Ethiopian rift [*Corti*, 2008]. These ridges are defined by large magmatic segments with a thicker lithosphere bordered by deeper avolcanic basins with a relatively thin lithosphere. The avolcanic segments at the SWIR are also characterised by either the presence of sediments or peridotitic rocks, a feature that we can only suspect in the Azores. The magmatic segments of the oceanic ridges typically consist of large volcanic structures, which, in the case of the Terceira Rift, form islands. As *Vogt and Jung* [2004] pointed out, the extreme topographic variation at the Terceira Rift is most likely the result of the presence of anomalous mantle beneath the Azores which led to the formation of a shallow oceanic plateau which is then divided by the Terceira Rift. A comparable segmentation pattern is also observed along the Mid-Atlantic Ridge from 25°N to 48°N [*Magde and Sparks*, 1997], where neither temperature differences nor viscosity changes have been found to affect the segmentation pattern. Instead, the ultraslow spreading may lead to an increased cooling beneath the avolcanic, hence cooler sections, forcing melts to laterally move along ridge, which produces the observed segmentation pattern [*Magde and Sparks*, 1997].

The degree of partial melting beneath the Terceira Rift is comparable or lower than at other ultraslow ridges but melting occurs much deeper, producing alkaline magmas in the Azores in contrast to mostly tholeiitic basalts at the Gakkel Ridge and the SWIR [e.g., *Michael et al.*, 2003; *Standish et al.*, 2008]. The process of conductive cooling becomes important at ultraslow spreading rates (<20 mm/a) leading to a decrease of melting at shallow depth and lower degrees of partial melting [*Reid and Jackson*, 1981]. As pointed out above, the smaller degrees of partial melting at the Terceira Rift are probably a result of the thicker surrounding lithosphere and the relatively recent transition from a transform fault to spreading (<6 Ma from $^{40}Ar/^{39}Ar$ age determinations) which lead to a thick lithospheric lid and deep melting. In contrast, spreading has been established for a long time at the Gakkel Ridge and SWIR leading to a thin lithosphere and shallow melting. The obliquity of ultraslow spreading rifts also has an important impact onto melting processes; i.e. an increasing obliquity leads to decreasing effective spreading rates, lower upwelling velocities and smaller melt fractions [*Okino et al.*, 2002; *Standish et al.*, 2008]. The spreading rate along the Terceira Rift increases from the east (3.7 mm/a) to the western edge (4.5 mm/a) and obliquity decreases from São Miguel (61°) to Graciosa (40° [*Vogt and Jung*, 2004]). We suggest that the smaller degrees of partial melting at the Terceira Rift compared to other ultraslow spreading rifts are a result of a combination of a thicker, relatively older lithosphere with a very slow spreading rate and a higher obliquity. The formation of islands along the axis, despite the smaller degrees of partial melting, results from the large relief amplitude of 2-4 km [*Vogt and Jung*, 2004] on a shallow plateau and is most likely the result of the presence of enriched and possibly hot mantle plume material beneath the rifted Azores Plateau. This material generates larger volumes of melts over longer time periods than the depleted mantle present beneath other ultraslow spreading axes. The distinct variations of melting degrees between the Terceira Rift volcanoes give either evidence for a limited melt production beneath the bathymetric basins or highly focused magmatism along-axis like it has been proposed for the SWIR [*Sauter et al.*, 2004b; *Standish et al.*, 2008] and the Ethiopian rift [*Corti*, 2008]. The occurrence of focused melts may also lead to increased melt volumes in the volcanic segments comparable to the oblique segment of the SWIR [*Standish et al.*, 2008]. As a result of the Oceanic Plateau situated in the vicinity of the spreading axis the Terceira Rift may indeed share many similarities with continental rifts (e.g. East African Rift system) such as low degrees of partial melting, oblique rifting and segmentation patterns.

The presence of well defined, distinct mantle sources beneath each island/seamount inferred from trace elements and Nd and Pb isotopes suggests that focused magmatism occurs along the Terceira Rift as has been proposed from geophysical observations along the SWIR and Ethiopian rift. The focusing most likely occurs in distinct mantle diapirs which underlie each volcanic system but lack beneath the avolcanic basins. Within the diapirs the melts are focussed to the surface and may mix within each diapir but not among different diapiric structures [*Crane*, 1985; *Okino et al.*, 2002]. The diapiric melts that have lower densities and viscosities than the surrounding mantle move towards regularly-spaced established gravitational instabilities of the partially molten mantle by porous flow avoiding mixing between the segments [*Lin et al.*, 1990; *Schouten et al.*, 1985; *Whitehead et al.*, 1984]. The initial establishment of gravitational melt instabilities is mainly controlled by the continuity and thickness of the underlying melt layer [*Crane*, 1985; *Michael et al.*, 2003], whereas the spacing of magmatic centres is mainly controlled by the effective spreading rate [*Schouten et al.*, 1985]. Slower spreading rates are correlated to smaller distances between the magmatic segments consistent with the relatively small scale segmentation pattern (10-30 km) observed along the Terceira Rift and other slow spreading rifts (e.g., Gakkel Ridge, SWIR) compared to faster spreading ridges such as the MAR (50-80 km). The segmentation pattern along the Terceira Rift is also comparable to propagating rifts such as the southern Iceland rift [*Tentler*, 2005] or continental rifts such as the East African Rift system [*Wright et al.*, 2006]. While a magmatic origin of the segmentation pattern beneath continental rifts is a matter of active debate (i.e. solely tectonic influences vs. magma intrusions [*Corti*, 2008 2347; *Wright et al.*, 2006]) the occurrence of segmentation patterns in oceanic rifts will most likely be controlled by the availability of melts [*Tentler*, 2005]. For the specific case of Iceland, the obliquity and segmentation pattern are likely to be controlled by the emplacement of dykes.

Summarising, the Terceira Rift represents an ultraslow spreading rift which consists of both continental (e.g. spreading rate, lithospheric thickness) and oceanic features (e.g. melt availability, segmentation pattern/focused magmatism). The Terceira Rift thus represents the first known ultraslow spreading rift within old (>10 Ma) oceanic lithosphere. It differs from other oceanic rifts mainly as a result of the lithospheric age and the presence of a melting anomaly and thus is a unique example of oceanic rifting. Based on the occurrence of both continental and oceanic features, one could speculate that the Terceira Rift may represent the earliest stages of a rift system and may later develop into an oceanic spreading centre.

CONCLUSIONS

We conclude that the melting depth along the Terceira Rift does not vary systematically beneath Graciosa, Terceira and João de Castro, where melts are generated in the spinel/garnet transition zone (Fig. 10). However, deeper melting in the garnet stability field is observed at São Miguel, the island most distant from the MAR and possibly with the thickest lithosphere. The degrees of partial melting are smaller at São Miguel and João de Castro compared to the other volcanic systems along the axis. Compared to other very slow spreading axes the generally low degrees of partial melting at the Terceira Rift probably result from a combination of a thick lithospheric lid and a relatively young (<1 Ma) and ultraslow spreading movement combined with a high obliquity (40° to 61°). Although the Terceira Rift has lower degrees of partial melting compared to the SWIR or Gakkel Ridge, the presence of an anomalous upper mantle generates enough melts over relatively long time periods to enable subaerial volcanism. The incompatible trace element ratios (e.g. Th/U, Nb/Zr) and combined Sr-Nd-Pb isotopes suggest that every volcanic system along the Terceira Rift is situated on a single binary mixing trend without evidence of mixing in between. The limited mixing is attributed to the presence of geochemical boundaries and the occurrence of focused magma transport in separate mantle diapirs as has been also observed on other ultraslow spreading rifts. The avolcanic–volcanic segmentation pattern along the Terceira Rift is comparable to the structures observed along the SWIR.

This implies that these segmentation patterns are characteristic features of ultraslow spreading rifts with spreading rates <14 mm/a. The Sr, Nd, and Pb isotope composition of Graciosa lavas and their relation to the isotope trend in MORB form the adjacent MAR suggest a mantle flux from Graciosa towards the MAR causing the observed enriched MORB compositions along the MAR.

ACKNOWLEDGEMENTS

We gratefully acknowledge the help of captain and crew of RV Poseidon for their help during the recovery of the samples. D. Garbe-Schönberg is thanked for the ICP-MS analyses. We also thank Steve J. Galer for his efforts and help with the triple spike Pb analyses and data correction. We gratefully acknowledge the constructive comments and reviews by V. Salters, E. Widom and an anonymous reviewer. C. Beier acknowledges inspiration by Dr. T. Coopers. C. Beier was funded by a Feodor Lynen fellowship of the Alexander von Humboldt Foundation during the final stages of the manuscript. This study has been funded by the Deutsche Forschungsgemeinschaft through grants Ha 2568/6-1, Ha 2568/9-2, and Ha 2100/7-1. This is GEMOC publication No. 5xx.

SUPPLEMENTARY MATERIAL

A supplemental, comprehensive dataset for this article can be found on the G^3-website.

LITERATURE

Abdel Monem, A. A., L. A. Fernandez, and G. M. Boone (1975), K-Ar-Ages from the eastern Azores group (Santa Maria, Sao Miguel and the Formigas islands), *Lithos*, *8*, 247-254.

Abouchami, W., S. J. G. Galer, and A. W. Hofmann (2000a), High precision lead isotope systematics of lavas from the Hawaiian Scientific Drilling Project, *Chem Geol*, *169*, 187-209.

Abouchami, W., A. W. Hofmann, and S. J. G. Galer (2000b), Lead Isotopic Evidence for Multiple Components in the Hawaiian Plume, paper presented at Goldschmidt Conference, Journal of Conference Abstracts, Oxford.

Baker, M. B., and E. M. Stolper (1994), Determining the composition of high-pressure mantle melts using diamond aggregates, *Geochim Cosmochim Acta*, *58*(13), 2811-2827.

Beattie, P. (1993), Uranium-thorium disequilibria and partitioning on melting of garnet peridotite, *Nature*, *363*(6424), 63-65.

Beier, C., K. M. Haase, and T. H. Hansteen (2006), Magma evolution of the Sete Cidades volcano, São Miguel, Azores, *J Petrol*, *47*, 1375-1411.

Beier, C., A. Stracke, and K. M. Haase (2007), The peculiar geochemical signatures of São Miguel lavas: metasomatised or recycled mantle sources?, *Earth Planet Sci Lett*, *259*(1-2), 186-199.

Blundy, J. D., T. J. Falloon, B. J. Wood, and J. A. Dalton (1995), Sodium partitioning between clinopyroxene and silicate melts, *J Geophys Res-Solid*, *100*(8), 15,501-515,515.

Bonatti, E. (1990), Not so hot "hot spots" in the oceanic mantle, *Science*, *250*(4977), 107-111.

Bougault, H., and Treuil (1980), Mid-Atlantic Ridge: zero age geochemical variations between Azores and 22°N, *Nature*, *286*, 209-212.

Bourdon, B., N. M. Ribe, A. Stracke, A. E. Saal, and S. P. Turner (2006), Insights into the dynamics of mantle plumes from uranium-series geochemistry, *Nature*, *444*(7120), 713-717.

Calvert, A. T., R. B. Moore, J. P. McGeehin, and A. M. Rodrigues da Silva (2006), Volcanic history and $^{40}Ar/^{39}Ar$ and ^{14}C geochronology of Terceira Island, Azores, Portugal, *J Volcanol Geoth Res*, *156*(1-2), 103-115.

Cannat, M., A. Briais, C. Deplus, J. Escartín, J. Georgen, J. Lin, S. Mercouriev, C. Meyzen, M. Muller, G. Pouliquen, A. Rabain, and P. d. Silva (1999), Mid-Atlantic Ridge - Azores hotspot interactions: along-axis migration of a hotspot-derived event of enhanced magmatism 10 to 4 Ma ago, *Earth Planet Sci Lett*, *173*, 257-269.

Cazenave, A. (1984), Thermal cooling of the oceanic lithosphere; new constraints from geoid height data, *Earth Planet Sci Lett*, *70*(2), 395-406.

Clague, D. A., W. S. Weber, and J. E. Dixon (1991), Picritic glasses from Hawaii, *Nature*, *353*, 553-556.

Cochran, J. R., G. J. Kurras, M. H. Edwards, and B. J. Coakley (2003), The Gakkel Ridge; bathymetry, gravity anomalies, and crustal accretion at extremely slow spreading rates, *J Geophys Res-Solid*, *108*(B2), doi:10.1029/2002JB001830.

Corti, G. (2008), Control of rift obliquity on the evolution and segmentation of the main Ethiopian rift, *Nature Geosci*, *1*(4), 258-262.

Courtillot, V., A. Davaille, J. Besse, and J. Stock (2003), Three distinct types of hotspots in the Earth´s mantle, *Earth Planet Sci Lett*, *205*, 295-308.

Crane, K. (1985), The spacing of rift axis highs; dependence upon diapiric processes in the underlying asthenosphere?, *Earth Planet Sci Lett*, *72*(4), 405-414.

Dick, H. J. B., and P. B. Kelemen (1990), Fractionation of Ti from rare earth elements during formation of harzburgite from lherzolite by magma/mantle interaction, *EOS Transaction, American Geophysical Union*, *72*, 545.

Dick, H. J. B., J. Lin, and H. Schouten (2003), An ultraslow-spreading class of ocean ridge, *Nature*, *426*(6965), 405-412.

Dosso, L., H. Bougault, C. Langmuir, C. Bollinger, O. Bonnier, and J. Etoubleau (1999), The age and distribution of mantle heterogeneity along the Mid-Atlantic Ridge (31-41°N), *Earth Planet Sci Lett*, *170*, 269-286.

Dupré, B., and C. J. Allegre (1983), Pb-Sr isotope variation in Indian Ocean basalts and mixing phenomena, *Nature*, *303*(5913), 142-146.

Ebinger, C. J., T. Yemane, G. Woldegabriel, J. L. Aronson, and R. C. Walter (1993), Late Eocene-Recent volcanism and faulting in the southern main Ethiopian rift, *Journal of the Geological Society*, *150*(1), 99-108.

Eggins, S. M. (1992), Petrogenesis of Hawaiian tholeiites; 1, Phase equilibria constraints, *Contrib Mineral Petrol*, *110*(2-3), 387-397.

Eisele, J., M. Sharma, S. J. G. Galer, J. Blichert-Toft, C. W. Devey, and A. W. Hofmann (2002), The role of sediment recycling in EM-1 inferred from Os, Pb, Hf, Nd, Sr isotope and trace element systematics of the Pitcairn hotspot, *Earth Planet Sci Lett*, *196*, 197-212.

Elliott, T., J. Blichert-Toft, A. Heumann, G. Koetsier, and V. Forjaz (2007), The origin of enriched mantle beneath Sao Miguel, Azores, *Geochim Cosmochim Acta*, *71*(1), 219-240.

Féraud, G., I. Kaneoka, and C. J. Allègre (1980), K/Ar Ages and Stress Pattern in the Azores: Geodynamic Implications, *Earth Planet Sci Lett*, *46*, 275-286.

Féraud, G., H.-U. Schmincke, J. Lietz, J. Gastaud, G. Pritchard, and U. Bleil (1981), New K-Ar ages, chemical analyses and magnetic data of rocks from the islands of Santa Maria (Azores), Porto Santo and Madeira (Madeira Archipelago) and Gran Canaria (Canary Islands), *Bulletin of Volcanology*, *44*, 359-375.

Galer, S. J. G., and R. K. O'Nions (1989), Chemical and isotopic studies of ultramafic inclusions from the San Carlos volcanic field, Arizona; a bearing on their petrogenesis, *J Petrol*, *30*(4), 1033-1064.

Galer, S. J. G., and W. Abouchami (1998), Practical application of lead triple spiking for correction of instrumental mass discrimination, in *V M Goldschmidt conference; extended abstracts*, edited, pp. 491-492, Mineralogical Society, London, United Kingdom.

Galer, S. J. G. (1999), Optimal double and triple spiking for high precision lead isotopic measurement, *Chem Geol*, *157*, 255-274.

Garbe-Schönberg, C.-D. (1993), Simultaneous determination of thirty-seven trace elements in twenty-eight international rock standards by ICP-MS, *Geostandards Newsletters*, *17*, 81-97.

Gast, P. W. (1968), Trace element fractionation and the origin of tholeiitic and alkaline magma types, *Geochim Cosmochim Acta*, *32*(10), 1057-1086.

Geshi, N., S. Umino, H. Kumagai, J. M. Sinton, S. M. White, K. Kisimoto, and T. W. Hilde (2007), Discrete plumbing systems and heterogeneous magma sources of a 24 km3 off-axis lava field on the western flank of East Pacific Rise, 14°S, *Earth Planet Sci Lett*, *258*(1-2), 61-72.

Grevemeyer, I. (1999), Isostatic geoid anomalies over mid-plate swells in the Central North Atlantic, *Journal of Geodynamics*, *28*(1), 41-50.

Grimison, N. L., and W. P. Chen (1986), The Azores-Gibraltar plate boundary; focal mechanisms, depths of earthquakes, and their tectonic implications, *J Geophys Res*, *B91*(2), 2029-2047.

Grimison, N. L., and W. P. Chen (1988), Source mechanisms of four Recent earthquakes along the Azores-Gibraltar plate boundary, *Geophysical Journal of the Royal Astronomical Society*, *92*(3), 391-401.

Haase, K. M. (1996), The relationship between the age of the lithosphere and the composition of oceanic magmas: Constraints on partial melting, mantle sources and the thermal structure of the plates, *Earth Planet Sci Lett*, *144*, 75-92.

Haase, K. M., and C. Beier (2003), Tectonic control of ocean island basalt sources on Sao Miguel, Azores?, *Geophys Res Lett*, *30*(16), 1856.

Hanan, B. B., and D. W. Graham (1996), Lead and helium isotope evidence from oceanic basalts for a common deep source of mantle plumes, *Science*, *272*(5264), 991-995.

Hart, S. R., E. H. Hauri, L. A. Oschmann, and J. A. Whitehead (1992), Mantle plumes and entrainment; isotopic evidence, *Science*, *256*(5056), 517-520.

Hart, S. R., and T. Dunn (1993), Experimental cpx/melt partitioning of 24 trace elements, *Contrib Mineral Petrol*, *113*, 1-8.

Harte, B., P. A. Winterburn, and J. J. Gurney (1987), Metasomatic phenomena in garnet peridotite facies mantle xenoliths from the Matsoku kimberlite pipe, Lesotho, in *Mantle Metasomatism*, edited by M. A. Menzies and C. J. Hawkesworth, pp. 145-220, Academic Press, London.

Hellebrand, E., and J. E. Snow (2003), Deep melting and sodic metasomatism underneath the highly oblique-spreading Lena Trough (Arctic Ocean), *Earth Planet Sci Lett*, *216*(3), 283-299.

Herzberg, C. (1995), Generation of plume magmas through time; an experimental perspective, *Chem Geol*, *126*(1), 1-16.

Herzberg, C., and M. J. O'Hara (1998), Phase equilibrium constraints on the origin of basalts, picrites, and komatiites, *Earth-Science Reviews*, *44*(1-2), 39-79.

Hirose, K., and I. Kushiro (1993), Partial melting of dry peridotites at high pressures; determination of compositions of melts segregated from peridotite using aggregates of diamond, *Earth Planet Sci Lett*, *114*(4), 477-489.

Hirose, K., and I. Kushiro (1998), Physics of the Earth and Planetary Interiors, *Magmatology; the role of magmas in the evolution of the Earth*, *107*(1-3), 111-118.

Hirschmann, M. M., and E. M. Stolper (1996), A possible role for garnet pyroxenite in the origin of the "garnet signature" in MORB, *Contrib Mineral Petrol*, *124*(2), 185-208.

Hirschmann, M. M., T. Kogiso, M. B. Baker, and E. M. Stolper (2003), Alkalic magmas generated by partial melting of garnet pyroxenite, *Geology*, *31*(6), 481-484.

Irving, A. J., and F. A. Frey (1978), Distribution of trace elements between garnet megacrysts and host volcanic liquids of kimberlitic to rhyolitic composition, *Geochim Cosmochim Acta*, *42*(6), 771-787.

Jaques, A. L., and D. H. Green (1980), Anhydrous melting of peridotite at 0–15 Kb pressure and the genesis of tholeiitic basalts, *Contrib Mineral Petrol*, *73*(3), 287-310.

Johnson, C. L., J. R. Wijbrans, C. G. Constable, J. Gee, H. Staudigel, L. Tauxe, V.-H. Forjaz, and M. Salgueiro (1998), $^{40}Ar/^{39}Ar$ ages and paleomagnetism of Sao Miguel lavas, Azores, *Earth Planet Sci Lett*, *116*(3-4), 637-649.

Johnson, K. T. M. (1994), Experimental cpx/ and garnet/ melt partitioning of REE and other trace elements at high pressures; petrogenetic implications, in *V M Goldschmidt Conference; extended abstracts*, edited, pp. 454-455, Mineralogical Society, London, United Kingdom.

Kane, K. A., and D. E. Hayes (1994), Long-lived mid-ocean ridge segmentation: Constraints on models, *J Geophys Res*, *99*(B10), 19,693-619,706.

Kelemen, P. B., N. Shimizu, and T. Dunn (1993), Relative depletion of niobium in some arc magmas and the continental crust; partitioning of K, Nb, La and Ce during melt/ rock reaction in the upper mantle, *Earth Planet Sci Lett*, *120*(3-4), 111-133.

King, S. D. (2007), Hotspots and edge-driven convection, *Geology*, *35*(3), 223-226.

Kogiso, T., K. Hirose, and E. Takahashi (1998), Melting experiments on homogeneous mixtures of peridotite and basalt: application to the genesis of ocean island basalts, *Earth Planet Sci Lett*, *162*(1-4), 45-61.

Krause, D. C., and N. D. Watkins (1970), North Atlantic crustal genesis in the vicinity of the Azores, *Geophys. Journ. Roy. Astron. Soc.*, *19*, 261-283.

Kushiro, I. (1996), Partial melting of a fertile mantle peridotite at high pressures: An experimental study using aggregates of diamond, in *Earth Processes: Reading the isotopic code*, edited, pp. 109-122, Am. Geophys. Union, Geophys. Monograph.

Le Maitre, R. (Ed.) (1989), *A classification of igneous rocks and glossary of terms, recommendations of the International union of geological sciences, subcomission on the systematics of igneous rocks.*, Blackwell, Oxford, London.

Leeman, W. P., and K. F. Scheidegger (1977), Olivine/ liquid distribution coefficients and a test for crystal-liquid equilibrium, *Earth Planet Sci Lett*, *35*(2), 247-257.

Lin, J., G. M. Purdy, H. Schouten, J. C. Sempere, and C. Zervas (1990), Evidence from gravity data for focused magmatic accretion along the Mid-Atlantic Ridge, *Nature*, *344*(6267), 627-632.

Macdonald, G. A. (1968), Composition and origin of Hawaiian lavas, in *Studies in volcanology--A memoir in honor of Howel Williams*, edited, pp. 477-522, Geological Society of America (GSA), Boulder, CO, United States.

MacDonald, K. C., D. S. Scheirer, and S. M. Carbotte (1991), Mid-ocean ridges; discontinuities, segments and giant cracks, *Science*, *253*(5023), 986-994.

Madeira, J., A. M. M. Soares, d. S. A. Brum, and A. Serralheiro (1995), Radiocarbon dating Recent volcanic activity on Faial Island (Azores), in *Proceedings of the 15th international radiocarbon conference*, edited, pp. 139-147, American Journal of Science, New Haven, CT, United States.

Madureira, P., M. Moreira, J. Mata, and C.-J. Allègre (2005), Primitive neon isotopes in Terceira Island (Azores archipelago), *Earth Planet Sci Lett*, *233*, 429-440.

Magde, L. S., and D. W. Sparks (1997), Three-dimensional mantle upwelling, melt generation, and melt migration beneath segment slow spreading ridges, *J Geophys Res-Solid*, *102*(9), 20,571-520,583.

Mattsson, H., and A. Hoskuldsson (2003), Geology of the Heimaey volcanic centre, south Iceland: early evolution of a central volcano in a propagating rift?, *J Volcanol Geoth Res*, *127*(1-2), 55-71.

Mattsson, H. B., and N. Oskarsson (2005), Petrogenesis of alkaline basalts at the tip of a propagating rift: Evidence from the Heimaey volcanic centre, south Iceland, *J Volcanol Geoth Res*, *147*(3-4), 245-267.

McDonough, W. F., and S.-S. Sun (1995), The composition of the Earth, *Chem Geol*, *120*, 223-253.

McKay, G. A. (1986), Crystal/liquid partitioning of REE in basaltic systems: Extreme fractionation of REE in olivine, *Geochim Cosmochim Acta*, *50*(1), 69-79.

McKee, E. H., and R. B. Moore (1992), Potassium-argon dates for trachytic rocks on Sao Miguel, Azores, *Isochron/West*.

McKenzie, D., and R. K. O'Nions (1991), Partial melt distributions from inversion of rare earth element concentrations, *J Petrol*, *32*(5), 1021-1091.

Michael, P. J., C. H. Langmuir, H. J. B. Dick, J. E. Snow, S. L. Goldstein, D. W. Graham, K. Lehnert, G. Kurras, W. Jokat, R. Mühe, and H. N. Edmonds (2003), Magmatic and amagmatic seafloor generation at the ultraslow-spreading Gakkel ridge, Arctic Ocean, *Nature*, *423*, 956-962.

Miranda, J. M., L. A. Mendes Victor, J. Z. Simoes, J. F. Luis, L. Matias, H. Shimamura, H. Shiobara, H. Nemoto, H. Mochizuki, A. Hirn, and J. C. Lépine (1998), Tectonic Setting of the Azores Plateau deduced from a OBS survey, *Marine Geophysical Researches*, *20*, 171-182.

Montelli, R., G. Nolet, F. A. Dahlen, G. Masters, E. R. Engdahl, and S. H. Hung (2004), Finite-frequency tomography reveals a variety of plumes in the mantle, *Science*, *303*(5656), 338-343.

Moreira, M., R. Doucelance, B. Dupre, M. Kurz, and C. J. Allegre (1999a), Helium and lead isotope geochemistry in the Azores Archipelago, in *European Union of Geosciences conference abstracts; EUG 10*, edited, p. 814, Cambridge Publications, Cambridge, United Kingdom.

Moreira, M., R. Doucelance, M. D. Kurz, B. Dupre, and C. J. Allegre (1999b), Helium and lead isotope geochemistry of the Azores Archipelago, *Earth Planet Sci Lett*, *169*(1-2), 189-205.

Niu, Y., and M. J. O'Hara (2008), Global Correlations of Ocean Ridge Basalt Chemistry with Axial Depth: a New Perspective, *J Petrol*, *49*(4), 633-644.

Nunes, J. C., V. H. Forjaz, J. L. Alves, and A. C. Bernardes (2003), Caracterização vulcanológica do Banco D. João de Castro (Açores): novos dados, *Ciências da Terra (UNL)*, *V*(CD-ROM), D55-D58.

Okino, K., D. Curewitz, M. Asada, K. Tamaki, P. Vogt, and K. Crane (2002), Preliminary analysis of the Knipovich Ridge segmentation; influence of focused magmatism and ridge obliquity on an ultraslow spreading system, *Earth Planet Sci Lett*, *202*(2), 275-288.

Onuma, N., H. Higuchi, H. Wakita, and H. Nagasawa (1968), Trace element partition between two pyroxenes and the host lava, *Earth Planet Sci Lett*, *5*(1), 47-51.

Prytulak, J., and T. Elliott (2007), TiO_2 enrichment in ocean island basalts, *Earth Planet Sci Lett*, *263*(3-4), 388-403.

Putirka, K. (1998), Garnet + liquid equilibrium, *Contrib Mineral Petrol*, *131*(2-3), 273-288.

Reid, I., and H. R. Jackson (1981), Oceanic spreading rate and crustal thickness, *Marine Geophysical Researches*, *5*(2), 165-172.

Ritsema, J., and R. M. Allen (2003), The elusive mantle plume, *Earth Planet Sci Lett*, *207*, 1-12.

Robinson, J. A. C., and B. J. Wood (1998), The depth of the spinel to garnet transition at the peridotite solidus, *Earth Planet Sci Lett*, *164*(1-2), 277-284.

Roeder, P. L., and R. F. Emslie (1970), Olivine-liquid equilibrium, *Contrib Mineral Petrol*, *29*, 275-289.

Salters, V. J. M., and J. Longhi (1999), Trace element partitioning during the initial stages of melting beneath mid-ocean ridges, *Earth Planet Sci Lett*, *166*(1-2), 15-30.

Salters, V. J. M., J. E. Longhi, and M. Bizimis (2002), Near mantle solidus trace element partitioning at pressures up to 3.4 GPa, *Geochem Geophys Geosys*, *3*(7), 10.1029/2001GC000148.

Sauter, D., H. Carton, V. Mendel, M. Munschy, J. C. Rommevaux, J. J. Schott, and H. Whitechurch (2004a), Ridge segmentation and magnetic structure of the Southwest Indian Ridge (at 50°30'E, 55°30'E and 66°20'E); implications for magmatic processes at ultraslow-spreading centers, *Geochemistry, Geophysics, Geosystems - G^3*, *5*, doi:10.1029/2003GC000581.

Sauter, D., V. Mendel, C. Rommevaux-Jestin, L. M. Parson, H. Fujimoto, C. Mével, M. Cannat, and K. Tamaki (2004b), Focused magmatism versus amagmatic spreading along the ultra-slow spreading Southwest Indian Ridge: Evidence from TOBI side scan imagery, *Geochem Geophys Geosys*, *5*(10), doi:10.1029/2004GC000738.

Scarfe, C. M., and D. J. Cronin (1986), Viscosity-temperature relationships of melts at 1 atm in the system diopside-albite, *American Mineralogist*, *71*(5-6), 767-771.

Schilling, J.-G. (1975), Azores mantle blob: rare-earth evidence, *Earth Planet Sci Lett*, *25*, 103-115.

Schilling, J.-G., M. B. Bergeron, and R. Evans (1980), Halogens in the mantle beneath the North Atlantic, *Philosophical Transactions of the Royal Society of London*, *A297*, 147-178.

Schouten, H., K. D. Klitgord, and J. A. Whitehead (1985), Segmentation of mid-ocean ridges, *Nature*, *317*(6034), 225-229.

Searle, R. C. (1980), Tectonic pattern of the Azores spreading center and triple junction, *Earth Planet Sci Lett*, *51*, 415-434.

Shaw, D. M. (1970), Trace element fractionation during anatexis, *Geochim Cosmochim Acta*, *34*, 237-243.

Silveira, G., E. Stutzmann, A. Davaille, J.-P. Montagner, L. Mendes-Victor, and A. Sebai (2006), Azores hotspot signature in the upper mantle, *J Volcanol Geoth Res*, *156*(1-2), 23-34.

Smith, M. C., M. R. Perfit, D. J. Fornari, W. I. Ridley, M. H. Edwards, G. J. Kurras, and K. L. Von Damm (2001), Magmatic processes and segmentation at a fast spreading mid-ocean ridge: Detailed investigation of an axial discontinuity on the East Pacific Rise crest at 9°37´N, *Geochem Geophys Geosys*, *2*.

Smith, W., and D. Sandwell (1997), Measured and estimated seafloor topography (version 4.2), World Data Center A for Marine Geology and Geophysics research publication RP-1.

Snyder, D. C., E. Widom, A. J. Pietruszka, R. W. Carlson, and H.-U. Schmincke (2007), Time scales of formation of zoned magma chambers: U-series disequilibria in the Fogo A and 1563 A.D. trachyte deposits, Sao Miguel, Azores, *Chem Geol*, *239*(1-2), 138-155.

Sobolev, A. V., and I. K. Nikogosian (1994), Petrology of long-lived mantle plume magmatism: Hawaii, Pacific and Reunion Island, Indian Ocean, *Petrology*, *2*, 111-144.

Standish, J., H. Dick, P. Michael, W. Melson, and T. O'Hearn (2008), MORB generation beneath the ultraslow spreading Southwest Indian Ridge (9-25°E): Major element chemistry and the importance of process versus source, *Geochemistry Geophysics Geosystems*, *9*(5), 39.

Stein, C. A., and S. Stein (1992), A model for the global variation in oceanic depth and heat flow with lithospheric age, *Nature*, *359*(6391), 123-129.

Stolz, A. J., and G. R. Davies (1988), Chemical and isotopic evidence from spinel lherzolite xenoliths for episodic metasomatism of the upper mantle beneath southeast Australia, *Journal of Petrology, Special Lithosphere Issue*, *29*, 303-330.

Stosch, H.-G. n. (1982), Rare earth element partitioning between minerals from anhydrous spinel peridotite xenoliths, *Geochim Cosmochim Acta*, *46*(5), 793-811.

Stracke, A., V. J. M. Salters, and K. W. W. Sims (1999), Assessing the presence of garnet-pyroxenite in the mantle sources of basalts through combined hafnium-neodymium-thorium isotope systematics, *Geochemistry, Geophysics, Geosystems - G 3*, *1*, doi:10.1029/1999GC000013.

Stracke, A., A. W. Hofmann, and S. R. Hart (2005), FOZO, HIMU and the rest of the mantle zoo, *Geochem Geophys Geosys*, *6*, doi:10.1029/2004GC000824.

Takahashi, E., and I. Kushiro (1983), Melting of a dry peridotite at high pressures and basalt magma genesis, *American Mineralogist*, *68*(9-10), 859-879.

Takahashi, E. (1986), Melting of a dry peridotite KLB-1 up to 14 GPa; implications on the origin of peridotitic upper mantle, in *Special section; Partial melting phenomena in the Earth and planetary evolution*, edited, pp. 9367-9382, American Geophysical Union, Washington, DC, United States.

Tentler, T. (2005), Propagation of brittle failure triggered by magma in Iceland, *Tectonophysics*, *406*(1-2), 17-38.

Udias, A., A. A. Lopez, and J. Mezcua (1976), Seismotectonic of the Azores-Alboran region, *Tectonophysics*, *31*(3-4), 259-289.

Vogt, P. R., and W. Y. Jung (2004), The Terceira Rift as hyper-slow, hotspot-dominated oblique spreading axis: A comparison with other slow-spreading plate boundaries, *Earth Planet Sci Lett*, *218*, 77-90.

Walter, M. J. (1998), Melting of garnet peridotite and the origin of komatiite and depleted lithosphere, *J Petrol*, *39*(1), 29-60.

White, W. M., S. R. Hart, and J. G. Schilling (1975), Geochemistry of the Azores and the Mid-Atlantic Ridge; 29 degrees N to 60 degrees N, *Year Book - Carnegie Institution of Washington*, *74*, 224-234.

White, W. M., J. G. Schilling, and S. R. Hart (1976), Evidence for the Azores mantle plume from strontium isotope geochemistry of the Central North Atlantic., *Nature*, *263*, 659-662.

White, W. M., M. D. M. Tapia, and J.-G. Schilling (1979), The Petrology and Geochemistry of the Azores Islands., *Contributions to Mineralogy and Petrology.*, *69*, 201-213.

Whitehead, J. A. J., H. J. B. Dick, and H. Schouten (1984), A mechanism for magmatic accretion under spreading centres, *Nature*, *312*(5990), 146-148.

Widom, E., R. W. Carlson, J. B. Gill, and H. U. Schmincke (1997), Th-Sr-Nd-Pb isotope and trace element evidence for the origin of the Sao Miguel, Azores, enriched mantle source, *Chem Geol*, *140*(1-2), 49-68.

Wright, T. J., C. Ebinger, J. Biggs, A. Ayele, G. Yirgu, D. Keir, and A. Stork (2006), Magma-maintained rift segmentation at continental rupture in the 2005 Afar dyking episode, *Nature*, *442*(7100), 291-294.

Zindler, A., and S. Hart (1986), Chemical Geodynamics, *Ann Rev Earth Planet Sc*, *14*, 493-571.

Figure Captions

Fig. 1. a) Bathymetric chart of the northern Azores platform and the Terceira Rift according to *Smith and Sandwell* [1997]. Orange dashed circle marks the assumed position of the plate triple junction and the dotted line is the estimated general trend of the Terceira Rift. Subaerial samples were taken on each of the three islands (for detailed sample locations see supplemental Table 1 and for São Miguel samples see *Beier et al.* [2006] and *Beier et al.* [2007]). Inset shows the major tectonic features in the Azores; the East Azores Fracture Zone (EAFZ) is the seismically inactive former plate boundary between the Eurasian and African Plates. The recent plate boundary is thought to be in the vicinity of the Terceira Rift. b) Depth profile along the Terceira Rift showing a segmentation pattern as also observed on other slow spreading ridges, such as the Arctic Gakkel Ridge [*Michael et al.*, 2003].

Fig. 2. Total alkalis (Na_2O+K_2O) versus SiO_2 on a volatile-free basis according to *Le Maitre* [1989]. The separation line between alkaline (AB) and tholeiitic compositions was taken from *Macdonald* [1968]. The fields of São Miguel and Terceira include subaerial and submarine samples. Major element data from São Miguel are from *Beier et al.* [2006]. Based on the bathymetry and geochemistry samples have been subdivided into four groups due to clarity: lavas from/around São Miguel, from/around Terceira, from/around Graciosa and from the João de Castro seamount (including lavas from the neighbouring Hirondelle Basin that are chemically comparable).

Fig. 3. Major element data versus MgO of the Terceira Rift samples. Fields show respective trends of the São Miguel and Terceira data. The most notable differences are observed in the FeO^T and K_2O contents (Fig. 3 c & e). Major element data from São Miguel are from *Beier et al*. [2006].

Fig. 4. Primitive mantle [*McDonough and Sun*, 1995] normalised trace element pattern of the Terceira Rift lavas. a) shows the islands of São Miguel and Terceira, b) shows samples from João de Castro and Graciosa.

Fig. 5. Trace element (a) La/Sm (chondrite normalised), (b) Rb/Nb and (c) Dy/Yb (chondrite normalised) ratios versus wt. % MgO of the Terceira Rift lavas, and (d) Nb/Zr versus Th/U ratios of the Terceira Rift lavas. Samples from Terceira and São Miguel are shown as fields to clarify the most notable differences among the Terceira Rift lavas. Chrondrite composition from *McDonough and Sun* [1995].

Fig. 6. Isotope systematics of the Terceira Rift lavas. MAR indicates samples from the Mid-Atlantic Ridge from *Dosso et al.* [1999]. Lines indicate linear arrays of São Miguel, Terceira, Graciosa and João de Castro, respectively. Pb triple spike analyses are marked with a white circle inside. The dashed circles represent possible mantle source end members for each mixing array. Arrow marks the trend towards the eastern São Miguel lavas discussed in *Beier et al.* [2007]

Fig. 7. Estimated primitive Al and Si compositions (see Table 2) from São Miguel, João de Castro, Terceira and Graciosa. Lavas from Heimaey, Reunion and Hawaii are shown for comparison [*Clague et al.*, 1991; *Eggins*, 1992; *Mattsson and Oskarsson*, 2005; *Sobolev and Nikogosian*, 1994]. Experimental data (peridotite) are from *Baker and Stolper* [1994], *Hirose and Kushiro* [1993], *Jaques and Green* [1980], *Kushiro* [1996], *Takahashi* [1986], *Takahashi and Kushiro* [1983] and *Walter* [1998]. Pyroxenitic melt experiments are from *Hirschmann et al.* [2003] and *Kogiso et al.* [1998].

Fig. 8. (a) Fractionation-corrected (12 wt.% MgO) Ti_{12} versus Na_{12} concentrations. The negative correlation of the Terceira Rift samples can best be explained by mixing an alkaline mantle source (e.g. an alkali basalt similar to sample SM18-8-97-5 from *Beier et al.* [2006]) and a depleted mantle source (Table 3, residual pyrolite source after 10% degree of partial melting). Degrees of partial melting correspond to the melting degrees inferred from the trace element ratios. (b & c) Primitive mantle normalised trace element ratios of (b) $(Ce/Y_b)_N$ versus $(C_{e)N}$ and (c) Primitive mantle normalised $(Dy/Y_b)_N$. Tick marks of melting curves represent 0.5%, 1%, 2%, 3%, 5%, and 6% batch partial melting [*Beier et al.*, 2007] of a an enriched mantle source with a trace element composition similar to those implied for the source of the western São Miguel lavas (Table 3).

Fig. 9. Mantle source systematics along the Terceira Rift showing variations in (a) fractionation-corrected (10 wt. % MgO) K-contents, Sm/Nd, Ba/Nb and Th/U ratios versus Nd isotope ratios (a & c) and $^{208}Pb^*/^{206}Pb^*$ (b & d) ratios. São Miguel and Terceira are shown as fields for clarity.

Fig. 10. Sketch illustrating the processes dominating the Terceira Rift evolution. The melting regions of Graciosa, João de Castro and Terceira are situated within the spinel/garnet transition zone. The São Miguel melts are generated within the garnet stability field. The mixing relationships described in the main text suggest only very limited mixing between each islands source. The occurrence a of a typical amagmatic – magmatic segmentation pattern has its origin in focused magmatism comparable to the SWIR. The isotope systematics suggest a mantle flux from Graciosa towards the adjoining MAR. Not to scale.

TABLE CAPTIONS

Tab. 1. Selected major element, trace element and Sr-Nd-Pb isotope data of whole rocks and glasses from the Terceira Rift. Major element, trace element and isotopic data from São Miguel are presented in *Beier et al.* [2006]. The whole-rock (WR) major element data were determined by XRF and the trace element data were determined by ICP-MS. Melting depth were calculated using fractionation corrected SiO_2 contents and the equation of *Haase* [1996]. The $^{232}Th/^{238}U$ ratios have been calculated from the trace element concentrations.

Tab. 2. Estimated primitive magma compositions from João de Castro, Graciosa and Terceira calculated from the major element trends in Fig. 3. Primary melt for São Miguel is sample SM0140 from *Beier et al.* [2006]. Only lavas with MgO >5wt.% have been taken into consideration to avoid extended crystal fractionation. Primary melts have been estimated to have Mg# of 72 in equilibrium with Fo89 [*Roeder and Emslie*, 1970].

Tab. 3. Melting conditions for Figure 8. Note that Ce, Yb and Dy have been normalised in Figure 8. Pyrolite composition from *McDonough and Sun* [1995]. Residual calculated for 10% degree of partial melting of pyrolite. Enriched source composition for Ce, Yb and Dy from western São Miguel [*Beier et al.*, 2007]. Representative enriched alkaline component is sample SM18-8-97-5 from *Beier et al.* [2006]. Partition coefficients for Ti were calculated by *McKenzie and O'Nions* [1991] after analyses from *Irving*[1978], *Harte et al.* [1987], *Stolz and Davies* [1988] and *Galer and O'Nions* [1989]. Na partition coefficients are from *Leeman and Scheidegger* [1977] for olivine, from *Blundy et al.* [1995] for Cpx, from *Onuma et al.* [1968] for Opx, and from *Putirka* [1998] for Grt. The partition coefficients for Ce, Yb and Dy are taken from *McKay* [1986] for olivine, *Kelemen et al.* [1993] and *Dick and Kelemen* [1990] for orthopyroxene, *Hart and Dunn* [1993] for clinopyroxene and *Stosch* [1982] for spinel. The garnet partition coefficients are from *Johnson* [1994]. Primitive upper mantle from *McDonough and Sun* [1995].

SUPPLEMENTAL MATERIAL

Supplemental Tab. 1. Comprehensive major element, trace element and Sr-Nd-Pb dataset of whole rocks and glasses from the Terceira Rift. Major element, trace element and isotopic data from São Miguel are presented in *Beier et al.* [2006]. The whole-rock (WR) major element data were determined by XRF and the trace element data were determined by ICP-MS. Major element data from glasses were determined by electron micropobe (EPMA). Melting depth were calculated using fractionation corrected SiO_2 contents and the equation of *Haase* [1996]. The $^{232}Th/^{238}U$ ratios have been calculated from the trace element concentrations.

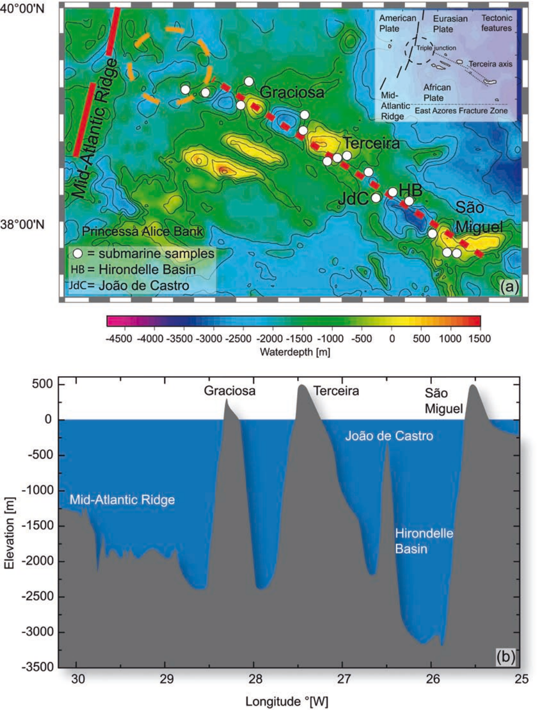

Beier et al., Figure 1

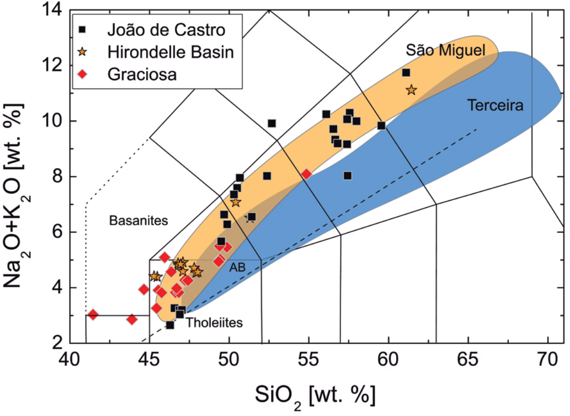

Beier et al.
Figure 2

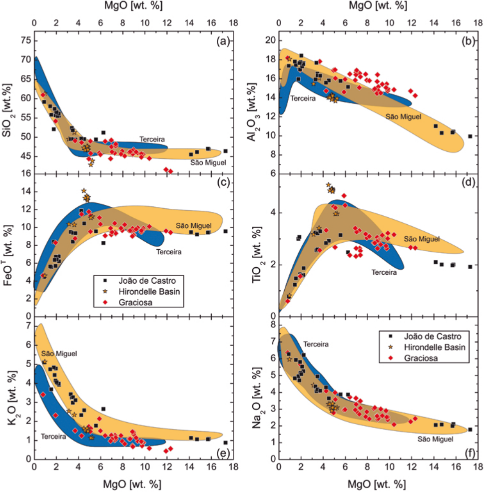

MgO [wt. %]
SiO2 [wt.%]
Terceira
São Miguel
(a)
Al2O3 [wt.%]
(b)
FeO^T [wt. %]
(c)
TiO2 [wt. %]
(d)
K2O [wt. %]
(e)
Na2O [wt. %]
(f)
João de Castro
Hirondelle Basin
Graciosa

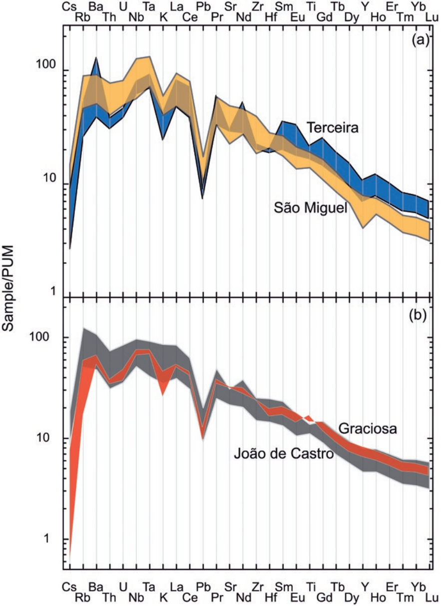

Beier et al.
Figure 4

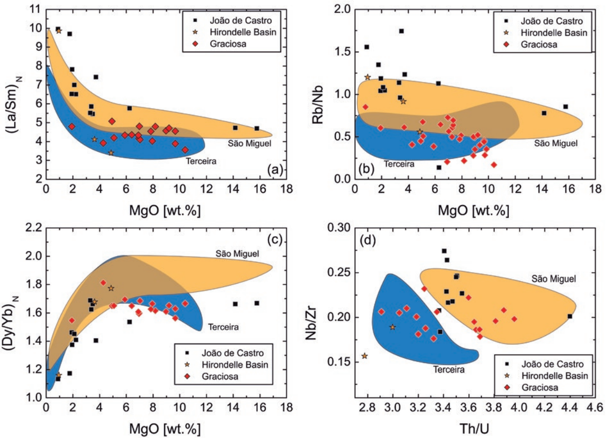

Beier et al.
Figure 5

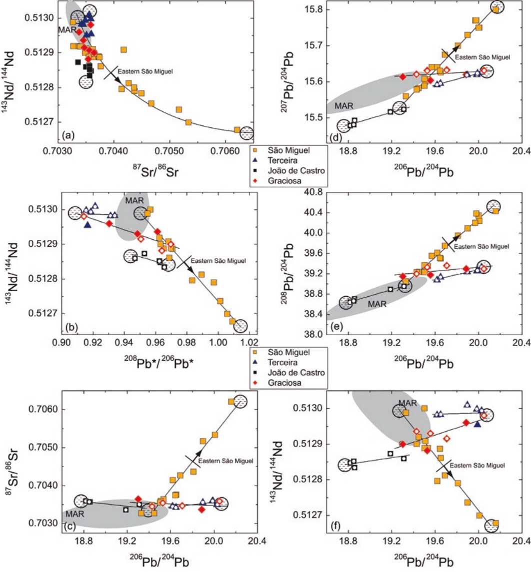

Beier et al.
Figure 6

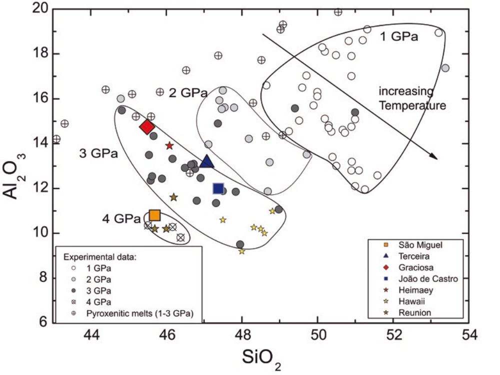

20
18
16
14
12
10
8
6
44
46
48
50
52
54
Al_2O_3
SiO_2
1 GPa
2 GPa
3 GPa
4 GPa
increasing
Temperature
Experimental data:
1 GPa
2 GPa
3 GPa
4 GPa
Pyroxenitic melts (1-3 GPa)
São Miguel
Terceira
Graciosa
João de Castro
Heimaey
Hawaii
Reunion

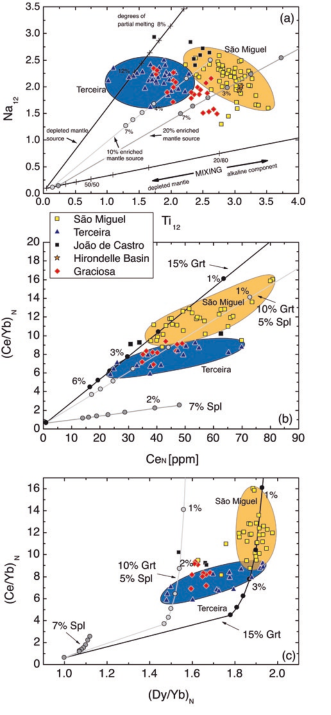

(a)
degrees of partial melting
8%
12%
4%
7%
3%
São Miguel
Terceira
depleted mantle source
20% enriched mantle source
10% enriched mantle source
20/80
50/50
MIXING
depleted mantle
alkaline component
Na12
Ti12
São Miguel
Terceira
João de Castro
Hirondelle Basin
Graciosa
15% Grt
1%
3%
6%
2%
10% Grt
5% Spl
7% Spl
(b)
(Ce/Yb)N
CeN [ppm]
(c)
(Dy/Yb)N

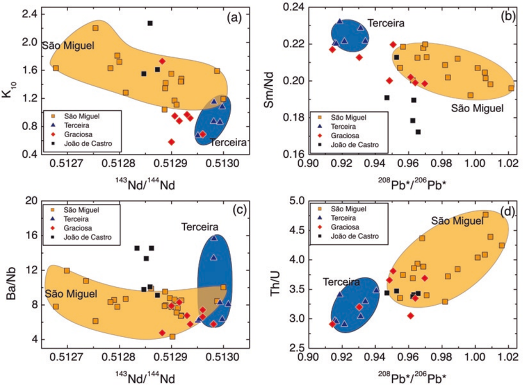

Beier et al.
Figure 9

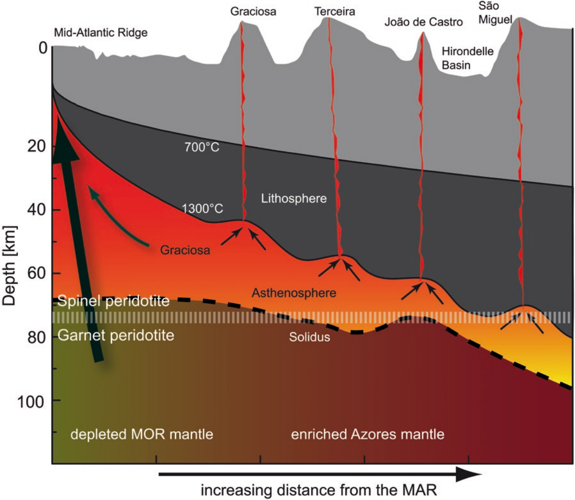

Beier et al.
Figure 10

Table 1 (Sample). Selected Major Element, Trace Element, and Sr-Nd-Pb Isotope Data of Whole Rocks and Glasses From the Terceira Rift[a] [The full Table 1 is available in the HTML version of this article at http://www.g-cubed.org]

Sample	513DS-1	515DS-1	523DS-1	524DS-2	525DS-2	558DS-1	558DS-8	542DS-1	244 DS-1	245 DS-4
Location	W slope of São Miguel	W slope of São Miguel	Banco João de Castro	Banco João de Castro	Banco João de Castro	Banco João de Castro	Banco João de Castro	SW Graciosa	W of Graciosa	(W of Graciosa)
Latitude (°N)	37°51.933N	37°51.874N	38°10.455N	38°11.287N	38°11.746N	38°13.725N	38°13.725N	39°05.966N	39°10.026N	39°08.184N
Longitude (°W)	25°56.277W	25°59.887W	26°37.895W	26°36.761W	26°35.852W	26°39.068W	26°39.068W	28°16.412W	28°17.959W	28°14.311W
Whole Rock/GL	Whole Rock	Whole Rock	Whole Rock	Glass	Whole Rock	Glass	Glass	Whole Rock	Glass	Whole Rock
TAS classification	Basalt	Trachyandesite	Trachyandesite	Basaltic Trachyandesite	Basalt	Trachyandesite	Basaltic Trachyandesite	Basalt	Basalt	Basalt
Melting depths (GPa)	2.65				2.67		1.57	3.17	3.08	3.57
(wt. %)										
SiO_2	46.95	59.29	55.58	52.39	46.89	56.70	49.42	45.76	45.98	44.85
TiO_2	2.74	1.28	1.87	2.56	2.01	1.56	3.29	2.73	4.66	2.73
Al_2O_3	12.33	18.69	17.64	17.67	10.45	17.75	16.33	15.10	14.60	15.07
Fe_2O_3	11.06	5.93	6.90	9.41	10.55	6.66	9.25	10.54	12.35	10.74
MnO	0.17	0.19	0.18	0.20	0.15	0.25	0.19	0.16	0.15	0.17
MgO	12.13	1.58	2.24	3.39	15.78	1.95	3.73	9.67	5.88	9.67
CaO	10.97	3.53	4.64	6.91	11.73	3.50	7.82	11.09	11.62	10.11
Na_2O	2.56	5.99	6.22	4.07	2.10	5.16	4.10	2.85	2.95	2.90
K_2O	1.38	4.32	3.93	3.25	1.09	4.78	3.12	0.91	2.14	0.95
P_2O_5	0.48	0.38	0.59	0.76	0.33	0.40	0.90	0.39	0.82	0.49
LOI	-	-	-	-	-	-	-	-	-	1.87
Total	100.77	101.18	99.79	100.63	101.08	98.71	98.15	99.20	101.16	97.68
(ppm)										
Sc	24.1	3.16	7.53	11.2	38.6	2.97	3.41	28.2	30.2	29.5
Cr	996	2.25	1.49	5.01	845	6.57	1.82	465	132	433
Co	44.6	4.95	7.85	16.3	59.4	6.67	6.77	38.9	48.8	45.4
Ni	319	1.75	-	5.94	376	0.10	-	182	100	183
Cu	70.5	3.29	5.37	16.3	162	4.40	3.95	42.2	45.9	46.1
Zn	90.0	92.1	103	112	84.8	111	107	103	114	91.9
Mo	1.90	0.97	4.63	3.65	1.29	5.42	4.93	1.39	-	-
-	-	-	-	-	-	-	-	-	-	-
Rb	28.5	1090	101	77.8	27.2	118	108	15.4	22.3	20.1
Sr	622	543	593	776	391	847	766	491	684	521
Y	19.3	33.7	41.8	36.8	18.2	38.2	36.6	20.3	26.1	26.4
Zr	259	607	447	296	146	376	476	172	279	222
Nb	48.0	130	96.8	81.0	31.8	99.2	87.4	33.7	57.5	45.6
Cs	0.32	0.26	0.82	0.61	0.23	0.92	0.86	0.19	0.21	0.26
Ba	404	-	976	792	290	1442	1165	280	275	263

[a] Major element, trace element, and isotopic data from São Miguel are presented by *Beier et al.* [2006]. The whole-rock (WR) major element data were determined by XRF and the trace element data were determined by ICP-MS. Melting depths were calculated using fractionation corrected SiO_2 contents and the equation of *Haase* [1996]. The $^{232}Th/^{238}U$ ratios have been calculated from the trace element concentrations.

Island	São Miguel	João de Castro	Graciosa	Terceira
SiO_2	45.7	47.6	45.6	47.3
TiO_2	2.7	2.6	2.1	2.1
Al_2O_3	10.8	12.0	14.9	13.8
FeO	10.2	9.5	9.5	9.3
MnO	0.2	0.2	0.2	0.2
MgO	12.7	12.3	12.5	11.8
CaO	12.0	11.3	11.0	11.3
Na_2O	2.2	2.6	2.1	2.4
K_2O	1.1	1.4	0.8	1.0
P_2O_5	0.4	0.4	0.5	0.3
Total	98.0	99.9	99.2	99.5

Tab. 2. Estimated primitive magma compositions from João de Castro, Graciosa and Terceira calculated from the major element trends in Fig. 3. Primary melt for São Miguel is sample SM0140 from Beier et al. [2006]. Only lavas with MgO >5wt.% have been taken into consideration to avoid extended crystal fractionation. Correction has been done either using a linearMg# 72.

	Source compositions (Fig. 8a)				Fig. 8b and c		Modal
	Pyrolite residual after 10% melting	Alkaline component	10% enriched source (Fig. 8a)	20% enriched source (Fig. 8a)	enriched source (Fig. 8)		**Spinel-peridodite**
Ti [ppm]	419	35,908	906	1,512	-	**olivine**	50%
Na [ppm]	779	4,076	912	1,079	-	**orthopyroxene**	20%
Ce [ppm]	-	-	-	-	1.50	**clinopyroxene**	15%
Yb [ppm]	-	-	-	-	0.69	**spinel**	15%
Dy [ppm]	-	-	-	-	0.99	**garnet**	-

Table 3: Melting conditions for Figure 8. Note that Ce, Yb and Dy have been normalised in Figure 8. Pyrolite Residual calculated for 10% degree of partial melting of pyrolite. Enriched source composition for Ce, Yb and Dy 1995]. Representative enriched alkaline component is sample SM18-8-97-5 from Beier et al. [2007]. Partition co O'Nions [2006] after analyses from Irving[1991], Harte et al. [1978], Stolz and Davies [1987] and Galer and C Leeman and Scheidegger [1989] for olivine, from Blundy et al. [1977] for Cpx, from Onuma et al. [1995] for Op coefficients for Ce, Yb and Dy are taken from McKay [1998] for olivine, Kelemen et al. [1986] and Dick and Ke [1990] for clinopyroxene and Stosch [1993] for spinel. The garnet partition coefficients are from Johnson [1982]. F [1994]

l composition of mantle sources (Fig. 8)

50:50 peridotite/pyroxenite mix, spinel/garnet transition	50:50 peridotite/pyroxenite mix, garnet stability
30%	30%
25%	25%
30%	30%
5%	-
10%	15%

: composition from McDonough and Sun [2006]. ' from western São Miguel [McDonough and Sun, efficients for Ti were calculated by McKenzie and)'Nions [1988]. Na partition coefficients are from ɔx, and from Putirka [1968] for Grt. The partition ɜlemen [1993] for orthopyroxene, Hart and Dunn ᴾrimitive upper mantle from McDonough and Sun

Auxiliary Material Submission for Paper 2008GC002112

Magma genesis by rifting of oceanic lithosphere above anomalous mantle: the Terceira Rift, Azores

Christoph Beier*
Max-Planck-Institut für Chemie (Otto-Hahn-Institut), Abteilung Geochemie, Postfach 3060, 55128 Mainz, Germany;
Institut für Geowissenschaften, Christian-Albrechts-Universität zu Kiel, Ludewig-Meyn-Straße 10, 24118 Kiel, Germany;
National Key Centre for Geochemical Evolution and Metallogeny of Continents (GEMOC), Department of Earth and Planetary Sciences, Macquarie University, NSW 2109, Sydney, Australia, Email: cbeier@els.mq.edu.au
Karsten M. Haase
GeoZentrum Nordbayern, Universität Erlangen, Schlossgarten 5, D-91054 Erlangen, Germany
Wafa Abouchami
Max-Planck-Institut für Chemie (Otto-Hahn-Institut), Abteilung Geochemie, Postfach 3060, 55128 Mainz, Germany
Marc-S. Krienitz
Institut für Geowissenschaften, Christian-Albrechts-Universität zu Kiel, Ludewig-Meyn-Straße 10, 24118 Kiel, Germany;
GeoForschungsZentrum Potsdam, Telegrafenberg B124, 14473 Potsdam, Germany
Folkmar Hauff
IFM-GEOMAR, Leibniz-Institut für Meereswissenschaften, Wischhofstr. 1-3, 24148 Kiel, Germany

*corresponding author, present address: National Key Centre for Geochemical Evolution and Metallogeny of Continents (GEMOC), Department of Earth and Planetary Sciences, Macquarie University, NSW 2109, Sydney, Australia, Tel.: +61/2/9850-4405, Fax.: +61/2/9850-8943, Email: cbeier@els.mq.edu.au

Geochemistry, Geophysics, Geosystems
doi:XXXXXXXXXXXXX

Abstract
This supplemental material consists of the comprehensive major element, trace element and Sr-nd-

Table Heading
Comprehensive major element, trace element and Sr-Nd-Pb dataset of whole rocks and glasses from the Terceira Rift. Major element, trace element and isotopic data from São Miguel are presented in Beier et al. [2006] and Beier et al. [2007]. The whole-rock (WR) major element data were determined by XRF and the trace element data were determined by ICP-MS. Major element data from glasses were determined by electron micropobe (EPMA). Melting depth were calculated using fractionation corrected SiO2 contents and the equation of Haase [1996]. The 232Th/238U ratios have been calculated from the trace element concentrations.

Beier, C., K. M. Haase, and T. H. Hansteen (2006), Magma evolution of the Sete Cidades volcano, São Miguel, Azores, J Petrol, 47, 1375-1411.

Beier, C., A. Stracke, and K. M. Haase (2007), The peculiar geochemical signatures of São Miguel lavas: metasomatised or recycled mantle sources?, Earth Planet Sci Lett, 259(1-2), 186-199.

Haase, K. M. (1996), The relationship between the age of the lithosphere and the composition of oceanic magmas: Constraints on partial melting, mantle sources and the thermal structure of the plates, Earth Planet Sci Lett, 144, 75-92.

Sample	513DS-1	515DS-1	523DS-1	524DS-2	525DS-2
Location	W slope of São Miguel	W slope of São Miguel	Banco João de Castro	Banco João de Castro	Banco João de Castro
Latitude [°N]	37°51.933N	37°51.874N	38°10.455N	38°11.287N	38°11.746N
Longitude [°W]	25°56.277W	25°59.887W	26°37.895W	26°36.761W	26°35.852W
Whole Rock/GL	Whole Rock	Whole Rock	Whole Rock	Glass	Whole Rock
TAS classification	Basalt	Trachyandesite	Trachyandsite	Basaltic Trachyandesite	Basalt
Melting depths [GPa]	2.65				2.67
[wt. %]					
SiO_2	46.95	59.29	55.58	52.39	46.89
TiO_2	2.74	1.28	1.87	2.56	2.01
Al_2O_3	12.33	18.69	17.64	17.67	10.45
Fe_2O_3	11.06	5.93	6.90	9.41	10.55
MnO	0.17	0.19	0.18	0.20	0.15
MgO	12.13	1.58	2.24	3.39	15.78
CaO	10.97	3.53	4.64	6.91	11.73
Na_2O	2.56	5.99	6.22	4.07	2.10
K_2O	1.38	4.32	3.93	3.25	1.09
P_2O_5	0.48	0.38	0.59	0.76	0.33
LOI	-	-	-	-	-
Total	100.77	101.18	99.79	100.63	101.08
[ppm]					
Sc	24.1	3.16	7.53	11.2	38.6
Cr	996	2.25	1.49	5.01	845
Co	44.6	4.95	7.85	16.3	59.4
Ni	319	1.75	-	5.94	376
Cu	70.5	3.29	5.37	16.3	162
Zn	90.0	92.1	103	112	84.8
Mo	1.90	0.97	4.63	3.65	1.29
-	-	-	-	-	-
Rb	28.5	1090	101	77.8	27.2
Sr	622	543	593	776	391
Y	19.3	33.7	41.8	36.8	18.2
Zr	259	607	447	296	146
Nb	48.0	130	96.8	81.0	31.8
Cs	0.32	0.26	0.82	0.61	0.23
Ba	404	-	976	792	290
La	36.6	89.5	72.5	67.4	24.1
Ce	75.5	173	137	131	49.2
Pr	9.51	19.4	15.9	15.7	5.98
Nd	38.3	68.0	58.5	60.8	24.1
Sm	7.93	11.8	11.2	11.5	5.13

Eu	2.43	3.32	3.17	3.27	1.53
Gd	6.70	9.65	9.39	9.29	4.61
Tb	0.96	1.44	1.36	1.31	0.65
Dy	5.16	7.76	7.75	7.20	3.61
Ho	0.93	1.44	1.46	1.30	0.66
Er	2.28	3.81	3.92	3.41	1.68
Tm	0.29	0.54	0.56	0.46	0.23
Yb	1.76	3.49	3.58	2.88	1.41
Lu	0.24	0.50	0.52	0.41	0.20
Hf	5.98	15.1	10.8	7.48	3.89
Ta	3.34	8.73	5.14	3.00	1.45
Pb	2.05	6.13	5.28	3.92	1.62
Th	3.82	13.5	8.79	7.32	2.51
U	1.14	1.76	2.56	2.15	0.72
			Pb triple spike	Pb triple spike	Pb triple spike
$^{87}Sr/^{86}Sr$	0.703273±8	0.703553±7	0.703498±8	0.703593±8	0.703361±8
$^{143}Nd/^{144}Nd$	0.512988±7	0.512888±5	0.512859±18	0.512847±4	0.512873±12
ε Nd	6.83	4.88	4.31	4.08	4.58
$^{206}Pb/^{204}Pb$	19.33±0.001	19.50±0.001	19.31±0.001	18.82±0.004	19.18±0.002
$^{207}Pb/^{204}Pb$	15.56±0.001	15.60±0.001	15.52±0.001	15.47±0.004	15.51±0.001
$^{208}Pb/^{204}Pb$	39.04±0.003	39.36±0.002	38.95±0.003	38.63±0.001	38.89±0.004
$^{208}Pb/^{206}Pb$	2.02	2.02	2.02	2.05	2.03
$^{208}Pb^*/^{206}Pb^*$	0.955	0.970	0.947	0.963	0.953
$^{232}Th/^{238}U$	3.46	7.91	3.55	3.52	3.59

558DS-1	558DS-8	542DS-1	244 DS-1	245 DS-4	249 DS-1
Banco João de Castro	Banco João de Castro	SW Graciosa	W of Graciosa	(W of Graciosa)	(W Riftzone of Graciosa)
38°13.725N 26°39.068W	38°13.725N 26°39.068W	39°05.966N 28°16.412W	39°10.026N 28°17.959W	39°08.184N 28°14.311W	39°06.356N 28°10.581W
Glass	Glass	Whole Rock	Glass	Whole Rock	Whole Rock
Trachyandesite	Basaltic Trachyandesite	Basalt	Basalt	Basalt	Trachybasalt
	1.57	3.17	3.08	3.57	1.91
56.70	49.42	45.76	45.98	44.85	48.63
1.56	3.29	2.73	4.66	2.73	3.33
17.75	16.33	15.10	14.60	15.07	14.73
6.66	9.25	10.54	12.35	10.74	12.76
0.25	0.19	0.16	0.15	0.17	0.21
1.95	3.73	9.67	5.88	9.67	4.27
3.50	7.82	11.09	11.62	10.11	8.24
5.16	4.10	2.85	2.95	2.90	4.08
4.78	3.12	0.91	2.14	0.95	1.25
0.40	0.90	0.39	0.82	0.49	1.01
-	-	-	-	1.87	0.32
98.71	98.15	99.20	101.16	97.68	98.51
2.97	3.41	28.2	30.2	29.5	19.9
6.57	1.82	465	132	433	19.0
6.67	6.77	38.9	48.8	45.4	26.6
0.10	-	182	100	183	13.0
4.40	3.95	42.2	45.9	46.1	9.44
111	107	103	114	91.9	147
5.42	4.93	1.39	-	-	-
-	-	-	-	-	-
118	108	15.4	22.3	20.1	26.0
847	766	491	684	521	717
38.2	36.6	20.3	26.1	26.4	46.4
376	476	172	279	222	309
99.2	87.4	33.7	57.5	45.6	63.6
0.92	0.86	0.19	0.21	0.26	0.24
1442	1165	280	275	263	368
86.6	80.4	25.6	34.2	31.4	49.1
159	151	55.1	83.8	67.5	104
18.0	17.0	7.24	10.0	8.64	14.1
64.3	60.8	30.0	39.5	34.2	57.7
11.1	10.8	6.59	7.87	6.90	12.5

3.29	3.12	2.10	2.48	2.17	4.05
8.80	8.63	5.90	6.74	6.18	11.6
1.27	1.21	0.89	0.99	0.92	1.71
6.96	6.79	5.09	5.31	5.05	9.26
1.31	1.27	0.97	0.95	0.92	1.66
3.57	„	2.49	2.42	2.40	4.12
0.50	0.49	0.33	0.32	0.33	0.54
3.29	3.14	2.03	2.03	2.10	3.32
0.48	0.47	0.29	0.28	0.30	0.45
9.59	11.3	5.32	6.35	4.98	7.14
4.35	4.39	2.47	3.38	2.54	3.53
5.41	4.94	1.78	1.96	2.19	2.36
10.4	9.58	2.69	3.48	3.37	4.52
3.04	2.84	0.71	1.04	1.10	1.55
Pb triple spike	Pb triple spike	Pb triple spike	Pb triple spike	Pb triple spike	Pb triple spike
0.703566±8	0.703565±3	0.703470±12	0.703543±12	0.703452±3	0.703582±3
0.512834±6	0.512851±5	0.512915±9	0.512882±4	0.512935±4	0.512980±7
3.82	4.17	5.40	4.76	5.81	6.69
18.86±0.001	18.85±0.002	19.70±0.001	19.52±0.002	19.42±0.002	20.04±0.001
15.49±0.001	15.48±0.003	15.63±0.001	15.63±0.003	15.62±0.002	15.63±0.002
38.70±0.005	38.66±0.001	39.35±0.003	39.32±0.010	39.20±0.006	39.29±0.006
2.05	2.05	2.00	2.01	2.02	1.96
0.966	0.963	0.951	0.964	0.961	0.914
3.54	3.49	3.94	3.46	3.15	3.01

AZG-03-07	AZG-03-28	529DS-4	535DS-7	AZT-03-11	AZT-03-12
South of Redondo, Graciosa	Road to Caldeira, Graciosa	E of Terceira	W flank Terceira	Coast at Cais dos Biscoitos, Terceira	Road Junction between Road 3-2 and 502, Terceira
39°04.210N	39°01.950N	38°32.614N	38°42.446N	38°47.960N	38°44.466N
28°04.250W	27°58.911W	26°52.509W	27°28.720W	27°15.830W	27°15.866W
Whole Rock	Whole Rock	Whole Rock	Whole Rock	Whole Rock	Whole Rock
Basalt	Basalt	Basalt	Basalt	Basalt	Basalt
3.43	2.96	2.81	2.95	2.65	2.65
45.17	46.24	46.57	46.27	46.95	46.95
3.10	3.27	1.90	3.86	3.02	3.88
15.80	16.89	14.54	14.96	13.81	13.92
11.48	10.55	9.62	13.31	11.95	13.79
0.16	0.15	0.15	0.18	0.17	0.21
8.17	7.02	10.55	6.15	8.25	5.45
10.70	10.50	10.23	10.58	10.51	9.48
2.42	2.86	2.90	3.22	3.21	3.65
0.82	1.08	1.10	0.85	0.93	1.29
0.45	0.46	0.38	0.46	0.85	1.31
1.13	-	-	-	-	-
98.27	99.02	97.94	99.84	99.65	99.93
33.0	27.2	26.2	-	27.6	23.3
334	222	539	92.0	301	64.0
48.5	42.2	35.1	-	40.9	31.4
137	108	205	72.0	116	27.8
39.3	28.3	48.0	-	35.5	22.6
89.7	89.2	77.0	109	95.1	118
1.27	1.33	4.21	-	1.30	1.39
-	-	-	-	-	-
9.24	23.0	22.2	24.0	19.0	27.2
590	639	414	593	529	536
25.9	25.6	18.1	-	32.0	42.7
237	224	136	272	178	216
42.4	40.7	27.0	-	37.0	48.4
0.02	0.18	0.25	-	0.16	0.24
335	303	324	-	496	756
32.1	26.5	21.5	-	34.9	49.0
69.0	58.2	44.4	-	79.0	112
8.62	7.53	5.62	-	10.2	14.2
33.7	30.3	22.7	-	44.2	61.3
6.68	6.45	5.07	-	10.1	13.6

2.13	2.13	1.64	-	3.82	4.79
6.20	6.05	4.80	-	9.71	12.9
0.87	0.86	0.74	-	1.37	1.80
4.73	4.67	4.43	-	7.49	9.79
0.86	0.84	0.86	-	1.34	1.74
2.25	2.16	2.24	-	3.33	4.29
0.30	0.29	0.30	-	0.43	0.54
1.90	1.80	1.87	-	2.59	3.31
0.27	0.25	0.27	-	0.35	0.45
4.49	5.02	4.21	-	4.59	5.40
2.47	2.39	1.85	-	2.52	3.15
1.66	1.46	2.08	-	1.15	1.59
2.86	2.47	2.35	-	2.16	3.03
0.77	0.77	0.68	-	0.71	0.92
				Pb triple spike	Pb triple spike
0.703647±3	0.703373±3	0.703519±10	0.703579±3	0.703454±2	0.703420±3
0.512897±3	0.512962±3	0.512866±10	0.512968±5	0.512981±3	0.512981±3
5.06	6.32	4.45	6.46	6.69	6.71
19.30±0.001	19.88±0.001	19.50±0.001	19.92±0.002	19.61±0.006	19.64±0.002
15.61±0.001	15.62±0.001	15.54±0.001	15.62±0.002	15.59±0.005	15.59±0.002
39.14±0.004	39.29±0.003	39.06±0.003	39.22±0.008	39.07±0.002	39.13±0.008
2.03	1.98	2.00	1.97	1.99	1.99
0.968	0.929	0.941	0.919	0.931	0.934
3.81	3.31	3.59	-	3.14	3.40

AZT-03-16	AZT-03-18	AZT-03-116	AZT-03-142	BHVO-1			BHVO-1
Pico do Gaspar, Terceira	E of Misterios dos Negors, Terceira	Cal Pedra, N flank of Santa Barbara, Terceira	Cerrado do Canto, Terceira	XRF		n=23	ICP-MS
38°53.830N 28°16.333W	38°44.001N 27°16.516W	38°46.333N 27°17.750W	38°45.916N 27°16.983W				
Whole Rock	Whole Rock	Whole Rock	Whole Rock	Standard		standard deviation	Standard
Basalt	Basaltic Trachyandesite	Basalt	Trachybasalt	Basalt			Basalt
2.78		2.74					
46.66	53.45	46.75	50.57	49.94	±	0.14	-
3.00	2.54	3.68	2.68	2.76	±	0.01	-
15.64	15.00	13.84	18.32	13.57	±	0.07	-
12.06	11.10	13.45	9.44	12.22	±	0.04	-
0.18	0.24	0.21	0.15	0.17	±	0.00	-
5.67	3.18	6.09	3.05	7.18	±	0.06	-
10.59	6.29	9.69	8.98	11.46	±	0.04	-
3.55	5.32	3.33	4.34	2.40	±	0.07	-
1.00	1.87	1.20	1.34	0.53	±	0.01	-
0.45	1.15	1.17	0.65	0.28	±	0.00	-
0.45	0.42	-	-	-	-	-	-
98.80	100.14	99.41	99.52	100.52	-	-	-
24.3	13.9	14.9	13.8	-	-	-	32.9
51.3	0.59	8.58	7.39	282	±	4.85	291
41.3	9.15	20.6	19.0	-	-	-	45.5
31.2	0.47	11.0	10.2	107	±	7.30	120
31.3	3.40	20.4	14.6	-	-	-	135
101	152	115	102	106	±	4.04	104
0.45	3.76	2.03	2.54	-	-	-	1.06
-	-	-	-	-	-	-	-
20.1	39.2	27.0	25.7	9.91	±	1.85	9.36
569	729	782	812	398	±	2.52	394
28.5	58.4	38.8	36.0	-	-	-	26.4
190	429	328	302	188	±	2.38	175
36.9	92.3	61.6	57.2	17.6	±	1.34	17.5
0.15	0.36	0.12	0.11	-	-	-	0.10
305	745	390	364	160	-	18.4	131
29.1	79.4	49.3	46.6	-	-	-	15.2
60.4	166	105	98.4	10.2	±	3.66	37.8
7.99	20.2	12.9	12.1	-	-	-	5.50
33.1	84.3	52.2	49.2	-	-	-	24.9
7.69	18.7	11.5	10.8	-	-	-	6.20

2.53	6.56	3.70	3.53	-	-	-	2.13
7.59	17.5	10.7	10.1	-	-	-	6.20
1.14	2.54	1.57	1.46	-	-	-	0.96
6.58	13.9	8.62	8.14	-	-	-	5.39
1.21	2.50	1.55	1.47	-	-	-	0.98
3.13	6.33	3.96	3.73	-	-	-	2.47
0.42	0.83	0.53	0.49	-	-	-	0.33
2.67	5.13	3.30	3.10	-	-	-	2.02
0.37	0.71	0.46	0.43	-	-	-	0.28
5.06	10.9	7.91	7.50	-	-	-	4.40
2.48	5.57	3.89	3.68	-	-	-	1.08
3.10	2.97	2.45	2.03	-	-	-	1.94
2.32	5.95	4.70	4.48	-	-	-	1.21
0.68	2.05	1.58	1.52	-	-	-	0.42
Pb triple spike	Pb triple spike	Pb triple spike	Pb triple spike				
0.703491±3	0.703556±3	0.703590±3	0.703592±3	-	-	-	-
0.512993±4	0.513009±6	0.512997±5	0.512953±4	-	-	-	-
6.93	7.24	7.01	6.16	-	-	-	-
20.02±0.002	19.89±0.002	19.98±0.003	19.98±0.002	-	-	-	-
15.62±0.003	15.61±0.003	15.61±0.004	15.62±0.002	-	-	-	-
39.32±0.001	39.23±0.001	39.25±0.015	39.26±0.009	-	-	-	-
1.96	1.97	1.96	1.96	-	-	-	-
0.919	0.921	0.916	0.916	-	-	-	-
3.52	3.00	3.07	3.05	-	-	-	-

n=12

	standard deviation		
-	-	-	-
-	-	-	-
-	-	-	-
-	-	-	-
-	-	-	-
-	-	-	-
-	-	-	-
-	-	-	-
-	-	-	-
-	-	-	-
-	-	-	-
-	-	-	-
±	1.54	-	-
±	9.84	-	-
±	1.95	-	-
±	4.54	-	-
±	9.81	-	-
±	4.22	-	-
±	0.09	-	-
-	-	-	-
±	0.30	-	-
±	12.7	-	-
±	1.29	-	-
±	6.47	-	-
±	0.46	-	-
±	0.00	-	-
±	2.54	-	-
±	0.38	-	-
±	0.58	-	-
±	0.07	-	-
±	0.31	-	-
±	0.13	-	-

±	0.06	-	-
±	0.20	-	-
±	0.03	-	-
±	0.15	-	-
±	0.04	-	-
±	0.08	-	-
±	0.01	-	-
±	0.07	-	-
±	0.01	-	-
±	0.08	-	-
±	0.04	-	-
±	0.23	-	-
±	0.09	-	-
±	0.02	-	-
-	-	-	-
-	-	-	-
-	-	-	-
-	-	-	-
-	-	-	-
-	-	-	-
-	-	-	-
-	-	-	-
-	-	-	-